CentAUR

Central Archive at the University of Reading

Reading's research outputs online

A mathematical model of the mevalonate cholesterol biosynthesis pathway

Frances Pool[a], Richard Currie[b], Peter K. Sweby[c], José Domingo Salazar[d], Marcus J. Tindall[c,e,*]

[a]*Institute of Ophthalmology, University College London, Gower Street, London, United Kingdom, WC1E 6BT.*

[b]*Syngenta, Jealott's Hill International Research Centre, Bracknell, Berkshire, United Kingdom, RG42 6EY.*

[c]*Department of Mathematics and Statistics, University of Reading, Whiteknights, Reading, United Kingdom, RG6 6AX.*

[d]*AstraZeneca, Unit 310, Cambridge Science Park, Milton Road, Cambridge, Cambridgeshire, United Kingdom, CB4 0FZ*

[e]*Institute of Cardiovascular and Metabolic Research, University of Reading, Whiteknights, Reading, United Kingdom, RG6 6AA.*

Abstract

We formulate, parameterise and analyse a mathematical model of the mevalonate pathway, a key pathway in the synthesis of cholesterol. Of high clinical importance, the pathway incorporates rate limiting enzymatic reactions with multiple negative feedbacks. In this work we investigate the pathway dynamics and demonstrate that rate limiting steps and negative feedbacks within it act in concert to tightly regulate intracellular cholesterol levels. Formulated using the theory of nonlinear ordinary differential equations and parameterised in the context of a hepatocyte, the governing equations are analysed numerically and analytically. Sensitivity and mathematical analysis demonstrate the importance of the two rate limiting enzymes 3-hydroxy-3-methylglutaryl-CoA reductase and squalene synthase in controlling the concentration of substrates within the pathway as well as that of cholesterol. The role of individual feedbacks, both global (between that of cholesterol and sterol regulatory element-binding protein 2; SREBP-2) and local internal (between substrates in the pathway) are investigated. We find that

whilst the cholesterol SREBP-2 feedback regulates the overall system dynamics, local feedbacks activate within the pathway to tightly regulate the overall cellular cholesterol concentration. The network stability is analysed by constructing a reduced model of the fall pathway and is shown to exhibit one real, stable steady-state. We close by addressing the biological question as to how farnesyl-PP levels are affected by CYP51 inhibition, and demonstrate that the regulatory mechanisms within the network work in unison to ensure they remain bounded.

1. Introduction

The mevalonate pathway is an important metabolic pathway present in all eukaryotes, fungi and some bacteria [6, 13]. It is responsible for many processes within the cell including biosynthesis of cholesterol, cell wall maintenance, hormone production, protein lipidation and anchoring and is part of steroid biosynthesis.

The body produces around 80% of cholesterol it needs [40]. A large percentage of this is synthesised by the liver via a series of reactions. In mammalian cells cholesterol is a substrate for a number of other reactions [6]. Over accumulation of cholesterol can lead to cellular toxicity [18], whilst insufficient cholesterol levels result in compromised cell structure and function. Thus it is important that cholesterol levels are tightly regulated within the cell. This is known as cellular cholesterol homeostasis and it works by balancing the influx, utilisation and efflux of cholesterol to maintain intracellular concentrations within a narrow range of concentration.

The mevalonate pathway is comprised of two genetic synthesis cascades which react with intermediate substrates to form cholesterol and has been comprehensively detailed by [22]. Sterol regulatory element-binding protein 2 (SREBP-2) co-regulates the gene transcription of 3-hydroxy-3-methylglutary coenzyme A reductase (HMGCR) and squalene synthase. This regulation is cholesterol dependent [13]. When cholesterol levels are high, SREBP-2 is bound in a complex with cholesterol anchoring it to the cell membrane rendering SREBP-2 inactive. In low cholesterol concentrations the complex

unbinds and through a complex series of translocation and proteolytic processing steps SREBP-2 is released, relocates to the nucleus and binds to target DNA stimulating increased transcription leading to increased production of the enzymes such as HMGCR and squalene synthase [6].

The central anabolic cascade of the pathway is initiated by the binding of HMGCoA to the active site of HMGCR, which then catalyses its conversion into mevalonate. Mevalonate is then converted to geranyl pyrophosphate (geranyl-PP), farnesyl pyrophosphate (farnesyl-PP), squalene (via the interaction between farnesyl-PP and squalene synthase), lanosterol and finally after some 19 further steps [11], cholesterol. A rate limiting step in this chain of biosynthesis is the reduction of HMGCoA catalysed by HMGCR [13].

The tight control of cholesterol concentration is thought possible by a number of negative feedback loops that regulate HMGCR and receptors dependent on intracellular cholesterol concentrations [14, 35]. Feedbacks from farnesyl-PP [10] and lanosterol accelerate HMGCR degradation [4], and it has been suggested that geranyl-PP plays a similar role. Cholesterol has been shown to accelerate squalene synthase degradation [10] and oxygenated derivatives of cholesterol have been identified in HMGCR degradation [9].

Many of the products formed from the mevalonate pathway are involved in other cell signalling cascades. Farnesyl-PP is a major branch point in the pathway which is responsible for producing six other substrates used in vital cellular functions. Excessive amounts of farnesyl-PP have been suggestively linked to tumours and Alzheimers disease [7, 32]. Inhibitors of the mevalonate pathway are used in cardiovascular therapy (statins) and as anti-fungal agents (CYP51 inhibitors) in crop protection. The extent to which altering this pathway is associated with the carcinogenic and developmental effects of CYP51 inhibitors has been debated [23, 26].

Mathematical modelling of cholesterol biosynthesis pathways has to date focused on specific aspects of the pathway. Kervizic and Corcos [19] developed a boolean model of the pathway which focused on demonstrating the role of SREBP-2 in synthesising cholesterol and the effect of statins on the process. Their model showed good agreement with experimental known functioning of the pathway in respect of statin applications. Watterson and colleagues [45] formulated an ordinary differential equation (ODE) model of the pathway to understand the effect of the immune response and statins on the overall

3

pathway. Using experimental data from macrophages, their work shows the gradual reduction in pathway activity as a result of the innate immune response, versus the more step like change imparted by statins. A recent paper by Bhattacharya et al. [2] formulated and analysed a three variable nonlinear ODE simplified model of the pathway that incorporates a description of HMGCR mRNA, HMGCR protein and cholesterol biosynthesis. The synthesis of HMGCR mRNA is controlled by a negative feedback loop, whereby cholesterol is able to bind to free SREBP-2. Model results and analysis demonstrate the system exhibits one real stable steady-state which is monotonic, periodic or damped periodic under certain model parameterisations as a result of cholesterol's negative regulation of SREBP-2.

In this paper we seek here to expand our knowledge of cholesterol biosynthesis by deriving and solving a nonlinear ODE model of the mevalonate cholesterol biosynthesis pathway. Our aim is to better understand the role of the overall network structure in dynamically regulating cholesterol biosynthesis, in particular that of multiple synthesis pathways and feedbacks. We begin in Section 2 by presenting our main model of the pathway which incorporates the core regulation mechanisms and feedbacks within the signalling cascade. An ODE model of the pathway is derived from first principles in Section 3, which is subsequently parameterised and solved numerically in Section 4. The results of a local sensitivity analysis are presented in Section 5 and the role of the second rate limiting step in the pathway between farnesyl-PP and squalene synthase is analysed in detail in Section 6. The effect of the numerous feedbacks within the pathway are analysed in Section 9 before a steady-state stability analysis of a model reduction of the full network model is presented in Section 7. Negative feedbacks may lead to a network exhibiting oscillatory type behaviour and as such we examine whether such solutions may be observed for certain parameterisations of the full model in Section 8. We test the hypothesis that the application of CYP51 inhibitors leads to increased levels of farnesyl-PP, via inhibition of cholesterol production following that of lanosterol, in Section 10. Our results and conclusions are discussed in Section 11.

2. The Mevalonate Pathway

Given the complexity of the full pathway we consider here a reduction, incorporating the details outlined in the Introduction, which captures the core

4

synthesis processes, feedbacks and branch points associated with cholesterol regulation as shown in Figure 1. Essentially, substrates and enzymes that form sequential linear steps in the pathway and which are not involved in feedbacks or branch points, have been omitted. This leaves three core aspects:

1. the two genetic transcriptional control pathways of HMGCR and squalene synthase by SREBP-2;

2. the central metabolic cascade which synthesises intermediary mevalonate products and sterols with controlling steps using the enzymes HMGCR and squalene synthase; and

3. negative feedback controls, including negative regulation of SREBP-2 by cholesterol and the concentration dependent feedbacks from sterol and non-sterol products affecting the HMGCR and squalene synthase degradation rates.

In high cholesterol concentrations SREBP-2 is bound to a cholesterol molecule anchoring it to the intracellular membrane, represented in Figure 1 by the $\bar{\kappa}_3/\bar{\kappa}_{-3}$ negative feedback. Here $\bar{\kappa}_3$ represents the association reaction, whilst $\bar{\kappa}_{-3}$ the disassociation reaction. In low cholesterol concentrations, SREBP-2 disassociates from the cholesterol molecule allowing it, via a series of intermediate steps, to produce an active transcription factor that relocates to the nucleus to act upon the DNA stimulating endogenous production of HMGCR and squalene synthase. This is represented in Figure 1, by the two reactions $\bar{\kappa}_1/\bar{\kappa}_{-1}$, through $\bar{\mu}_1$ to $\bar{\mu}_3$ and $\bar{\kappa}_2/\bar{\kappa}_{-2}$, through $\bar{\mu}_2$ to $\bar{\mu}_4$. In the centre of the pathway HMGCR binds with HMGCoA to form an intermediary complex which leads to mevalonate production. This is subsequently phosphorylated twice then converted to isopentenyl-PP and geranyl-PP. In Figure 1 these five steps are represented as $\bar{\mu}_5$. From geranyl-PP, farnesyl-PP is produced. It is at this point that squalene synthase reacts with farnesyl-PP and this complex produces squalene. Squalene produces squalene-2,3-epoxide after which lanosterol is formed. We represent these two steps by $\bar{\mu}_8$. There are a further 19 reactions from lanosterol until cholesterol [11] which we approximate by the parameter $\bar{\mu}_9$. This approximation allows for the simplification of an otherwise already under parameterised system.

There are a number of feedbacks within the pathway shown in Figure 1. Goldstein and Brown [4] found that sterols caused a negative feedback on HMGCR production but hypothesised sterols were not the only inhibitors.
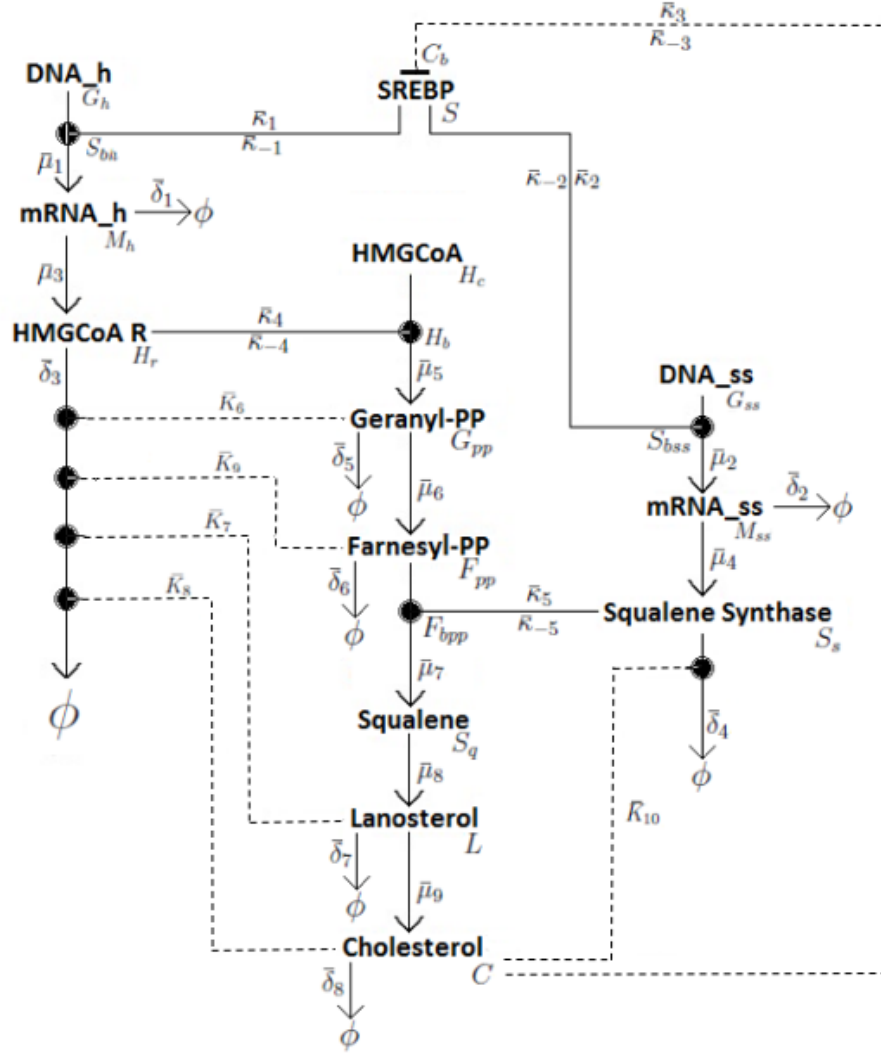
Figure 1: A simplified model of the mevalonate pathway. Arrows show forward reactions, circles show stimulative reactions and horizontal bars indicate inhibition. Here ϕ indicates the removal of a product from the pathway, either by degradation or use in another process. There are three main focal points to the pathway; the two genetic pathways of HMGCR and squalene synthase, the central metabolic cascade and the regulatory feedbacks (dashed lines).

Hence we have concentration dependent feedbacks from lanosterol ($\bar{K}_7$) and
cholesterol ($\bar{K}_8$) that up-regulate the degradation of HMGCR. It has been
suggested that geranyl-PP also up-regulates HMGCR degradation [14] ($\bar{K}_6$)
and recent findings by Foresti et al. [10] have shown farnesyl-PP is linked to
HMGCR degradation ($\bar{K}_9$). Foresti et al. also show a similar concentration
dependent reaction between cholesterol and the rate of squalene synthase
degradation ($\bar{K}_{10}$).

3. Mathematical model

In this section we derive a system of non-linear ODEs to describe the reaction
network detailed in Section 2 using the law of mass action. Details on the
biochemistry underlying each step within the pathway are given in Appendix
A. Applying the law of mass action to equations (A.1) - (A.6) gives

$$\frac{d\bar{g}_h}{d\bar{t}} = \bar{\kappa}_{-1}\bar{s}_{bh} - \bar{\kappa}_1\bar{s}^{x_h}\bar{g}_h, \tag{1}$$

$$\frac{d\bar{g}_{ss}}{d\bar{t}} = \bar{\kappa}_{-2}\bar{s}_{bss} - \bar{\kappa}_2\bar{s}^{x_s}\bar{g}_{ss}, \tag{2}$$

$$\frac{d\bar{s}}{d\bar{t}} = x_h\bar{\kappa}_{-1}\bar{s}_{bh} - x_h\bar{\kappa}_1\bar{s}^{x_h}\bar{g}_h + x_s\bar{\kappa}_{-2}\bar{s}_{bss} - x_s\bar{\kappa}_2\bar{s}^{x_s}\bar{g}_{ss} - \bar{\kappa}_3\bar{c}^{x_c}\bar{s} + \bar{\kappa}_{-3}\bar{c}_b, \tag{3}$$

$$\frac{d\bar{s}_{bh}}{d\bar{t}} = -\bar{\kappa}_{-1}\bar{s}_{bh} + \bar{\kappa}_1\bar{s}^{x_h}\bar{g}_h, \tag{4}$$

$$\frac{d\bar{s}_{bss}}{d\bar{t}} = -\bar{\kappa}_{-2}\bar{s}_{bss} + \bar{\kappa}_2\bar{s}^{x_s}\bar{g}_{ss}, \tag{5}$$

$$\frac{d\bar{m}_h}{d\bar{t}} = \bar{\mu}_1\bar{s}_{bh} - \bar{\delta}_1\bar{m}_h, \tag{6}$$

$$\frac{d\bar{m}_{ss}}{d\bar{t}} = \bar{\mu}_2\bar{s}_{bss} - \bar{\delta}_2\bar{m}_{ss}, \tag{7}$$

$$\frac{d\bar{h}_r}{d\bar{t}} = \bar{\mu}_3\bar{m}_h + \bar{\kappa}_{-4}\bar{h}_b - \bar{\kappa}_4\bar{h}_r\bar{h}_c + \bar{\mu}_5\bar{h}_b$$
$$- \bar{\delta}_3\bar{h}_r\left(1 + \delta_{hg}\frac{\bar{g}_{pp}}{\bar{g}_{pp} + \bar{K}_6} + \delta_{hf}\frac{\bar{f}_{pp}}{\bar{f}_{pp} + \bar{K}_9} + \delta_{hl}\frac{\bar{l}}{\bar{l} + \bar{K}_7} + \delta_{hc}\frac{\bar{c}}{\bar{c} + \bar{K}_8}\right), \tag{8}$$

$$\frac{d\bar{s}_s}{d\bar{t}} = \bar{\mu}_4\bar{m}_{ss} + \bar{\kappa}_{-5}\bar{f}_{bpp} - \bar{\kappa}_5\bar{s}_s\bar{f}_{pp}^2 + \bar{\mu}_7\bar{f}_{bpp} - \bar{\delta}_4\bar{s}_s\left(1 + \delta_{sc}\frac{\bar{c}}{\bar{c} + \bar{K}_{10}}\right), \tag{9}$$

7

$$\frac{d\bar{h}_c}{d\bar{t}} = \bar{\kappa}_{-4}\bar{h}_b - \bar{\kappa}_4\bar{h}_r\bar{h}_c + \bar{\omega}, \tag{10}$$

$$\frac{d\bar{h}_b}{d\bar{t}} = -\bar{\kappa}_{-4}\bar{h}_b + \bar{\kappa}_4\bar{h}_r\bar{h}_c - \bar{\mu}_5\bar{h}_b - \bar{\delta}_3\bar{h}_b, \tag{11}$$

$$\frac{d\bar{g}_{pp}}{d\bar{t}} = \bar{\mu}_5\bar{h}_b - \bar{\delta}_5\bar{g}_{pp} - \bar{\mu}_6\bar{g}_{pp}, \tag{12}$$

$$\frac{d\bar{f}_{pp}}{d\bar{t}} = \bar{\mu}_6\bar{g}_{pp} - \bar{\delta}_6\bar{f}_{pp} - 2\bar{\kappa}_5\bar{s}_s\bar{f}_{pp}^2 + 2\bar{\kappa}_{-5}\bar{f}_{bpp}, \tag{13}$$

$$\frac{d\bar{f}_{bpp}}{d\bar{t}} = \bar{\kappa}_5\bar{s}_s\bar{f}_{pp}^2 - \bar{\kappa}_{-5}\bar{f}_{bpp} - \bar{\mu}_7\bar{f}_{bpp} - \bar{\delta}_4\bar{f}_{bpp}, \tag{14}$$

$$\frac{d\bar{s}_q}{d\bar{t}} = \bar{\mu}_7\bar{f}_{bpp} - \bar{\mu}_8\bar{s}_q, \tag{15}$$

$$\frac{d\bar{l}}{d\bar{t}} = \bar{\mu}_8\bar{s}_q - \bar{\delta}_7\bar{l} - \bar{\mu}_9\bar{l}, \tag{16}$$

$$\frac{d\bar{c}}{d\bar{t}} = \bar{\mu}_9\bar{l} - \bar{\delta}_8\bar{c} + x_c\bar{\kappa}_{-3}\bar{c}_b - x_c\bar{\kappa}_3\bar{c}^{x_c}\bar{s}, \tag{17}$$

$$\frac{d\bar{c}_b}{d\bar{t}} = \bar{\kappa}_3\bar{c}^{x_c}\bar{s} - \bar{\kappa}_{-3}\bar{c}_b, \tag{18}$$

where, with square brackets denoting concentration,

$$\bar{g}_h = [G_h], \quad \bar{g}_{ss} = [G_{ss}], \quad \bar{s} = [S], \quad \bar{s}_{bh} = [S_{bh}], \quad \bar{s}_{bss} = [S_{bss}],$$
$$\bar{m}_h = [M_h], \quad \bar{m}_{ss} = [M_{ss}], \quad \bar{h}_r = [H_r], \quad \bar{s}_s = [S_s], \quad \bar{h}_c = [H_c],$$
$$\bar{h}_b = [H_b], \quad \bar{g}_{pp} = [G_{pp}], \quad \bar{f}_{pp} = [F_{pp}], \quad \bar{f}_{bpp} = [F_{bpp}], \quad \bar{s}_q = [S_q],$$
$$\bar{l} = [L], \quad \bar{c} = [C], \quad \text{and} \quad \bar{c}_b = [C_b],$$

and the system is closed with the initial conditions

$$\bar{g}_h(0) = \bar{g}_{h0}, \quad \bar{g}_s(0) = \bar{g}_{s0}, \quad \bar{s}(0) = \bar{s}_0, \quad \bar{s}_{bh}(0) = 0, \quad \bar{s}_{bss}(0) = 0,$$
$$\bar{m}_h(0) = \bar{m}_{h0}, \quad \bar{m}_{ss}(0) = \bar{m}_{ss0}, \quad \bar{h}_r(0) = \bar{h}_{r0}, \quad \bar{s}_s(0) = \bar{s}_{s0},$$
$$\bar{h}_c(0) = \bar{h}_{c0}, \quad \bar{h}_b(0) = 0, \quad \bar{g}_{pp}(0) = 0, \quad \bar{f}_{pp}(0) = 0, \quad \bar{f}_{bpp}(0) = 0,$$
$$\bar{s}_q(0) = 0, \quad \bar{l}(0) = 0, \quad \bar{c}(0) = 0 \quad \text{and} \quad \bar{c}_b(0) = 0, \tag{19}$$

at $\bar{t} = 0$

Many of the initial conditions are assumed equal to zero in order to understand the overall dynamical response of the system. The feedbacks acting

8

on HMGCR and squalene synthase degradation, equations (22) and (23) respectively, are dependent on geranyl-PP, farnesyl-PP, lanosterol and cholesterol concentrations. We thus assume these follow sigmoidal shape kinetics [24], where $\bar{K}_{6,7,8,9,10}$ are the respective Michaelis-Menten constants and $\delta_{hg}, \delta_{hf}, \delta_{hl}$ and δ_{hc}, are dimensionless weighting constants representing the additional effect of geranyl-PP, farnesyl-PP, lanosterol and cholesterol to that of the natural rate of HMGCR degradation, respectively, and δ_{sc} is that of a similar effect of cholesterol on the natural decay rate of squalene synthase.

By invoking conservation of certain entities within the pathway and employing quasi-equilibrium approximations (see Appendix B) equations (1) to (17) are reduced to

$$\frac{d\bar{m}_h}{d\bar{t}} = \frac{\bar{\mu}_1}{1 + \left(\frac{\bar{K}_1(1+(\frac{\bar{c}}{\bar{K}_3})^{x_c})}{\bar{s}_0}\right)^{x_h}} - \bar{\delta}_1 \bar{m}_h, \tag{20}$$

$$\frac{d\bar{m}_{ss}}{d\bar{t}} = \frac{\bar{\mu}_2}{1 + \left(\frac{\bar{K}_2(1+(\frac{\bar{c}}{\bar{K}_3})^{x_c})}{\bar{s}_0}\right)^{x_s}} - \bar{\delta}_2 \bar{m}_{ss}, \tag{21}$$

$$\frac{d\bar{h}_r}{d\bar{t}} = \bar{\mu}_3 \bar{m}_h + \bar{\kappa}_{-4} \bar{h}_b - \bar{\kappa}_4 \bar{h}_r \bar{h}_c + \bar{\mu}_5 \bar{h}_b$$
$$- \bar{\delta}_3 \bar{h}_r \left(1 + \delta_{hg} \frac{\bar{g}_{pp}}{\bar{g}_{pp} + \bar{K}_6} + \delta_{hf} \frac{\bar{f}_{pp}}{\bar{f}_{pp} + \bar{K}_9} + \delta_{hl} \frac{\bar{l}}{\bar{l} + \bar{K}_7} + \delta_{hc} \frac{\bar{c}}{\bar{c} + \bar{K}_8}\right), \tag{22}$$

$$\frac{d\bar{s}_s}{d\bar{t}} = \bar{\mu}_4 \bar{m}_{ss} + \bar{\kappa}_{-5} \bar{f}_{bpp} - \bar{\kappa}_5 \bar{s}_s \bar{f}_{pp}^2 + \bar{\mu}_7 \bar{f}_{bpp} - \bar{\delta}_4 \bar{s}_s \left(1 + \delta_{sc} \frac{\bar{c}}{\bar{c} + \bar{K}_{10}}\right), \tag{23}$$

$$\frac{d\bar{h}_c}{d\bar{t}} = \bar{\kappa}_{-4} \bar{h}_b - \bar{\kappa}_4 \bar{h}_r \bar{h}_c + \bar{\omega}, \tag{24}$$

$$\frac{d\bar{h}_b}{d\bar{t}} = -\bar{\kappa}_{-4} \bar{h}_b + \bar{\kappa}_4 \bar{h}_r \bar{h}_c - \bar{\mu}_5 \bar{h}_b - \bar{\delta}_3 \bar{h}_b, \tag{25}$$

$$\frac{d\bar{g}_{pp}}{d\bar{t}} = \bar{\mu}_5 \bar{h}_b - \bar{\delta}_5 \bar{g}_{pp} - \bar{\mu}_6 \bar{g}_{pp}, \tag{26}$$

$$\frac{d\bar{f}_{pp}}{d\bar{t}} = \bar{\mu}_6 \bar{g}_{pp} - \bar{\delta}_6 \bar{f}_{pp} - 2\bar{\kappa}_5 \bar{s}_s \bar{f}_{pp}^2 + 2\bar{\kappa}_{-5} \bar{f}_{bpp}, \tag{27}$$

$$\frac{d\bar{f}_{bpp}}{d\bar{t}} = \bar{\kappa}_5 \bar{s}_s \bar{f}_{pp}^2 - \bar{\kappa}_{-5} \bar{f}_{bpp} - \bar{\mu}_7 \bar{f}_{bpp} - \bar{\delta}_4 \bar{f}_{bpp}, \tag{28}$$

9

$$\frac{d\bar{s}_q}{d\bar{t}} = \bar{\mu}_7 \bar{f}_{bpp} - \bar{\mu}_8 \bar{s}_q, \tag{29}$$

$$\frac{d\bar{l}}{d\bar{t}} = \bar{\mu}_8 \bar{s}_q - \bar{\delta}_7 \bar{l} - \bar{\mu}_9 \bar{l}, \tag{30}$$

$$\frac{d\bar{c}}{d\bar{t}} = \frac{\bar{\mu}_9 \bar{l} - \bar{\delta}_8 \bar{c}}{1 - x_c(\bar{s}' + x_h \bar{s}'_{bh} + x_s \bar{s}'_{bss})}, \tag{31}$$

where $\bar{s}\prime_{bss}$, $\bar{s}\prime_{bh}$ and $\bar{s}\prime$ are given by equations (B.9), (B.10) and (B.8) respectively, and $\prime$ indicates differentiation with respect to $\bar{c}$. The initial conditions are given by

$$\bar{m}_h(0) = \bar{m}_{h0}, \quad \bar{m}_{ss}(0) = \bar{m}_{ss0}, \quad \bar{h}_r(0) = \bar{h}_{r0}, \quad \bar{s}_s(0) = \bar{s}_{s0},$$
$$\bar{h}_c(0) = \bar{h}_{c0}, \quad \bar{h}_b(0) = 0, \quad \bar{g}_{pp}(0) = 0, \quad \bar{f}_{pp}(0) = 0, \quad \bar{f}_{bpp}(0) = 0,$$
$$\bar{s}_q(0) = 0, \quad \bar{l}(0) = 0 \quad \text{and} \quad \bar{c}(0) = 0. \tag{32}$$

3.1. Non-dimensionalisation

Equations (20) to (32) are non-dimensionalised according to the following rescalings

$$\bar{t} = \frac{t}{\delta_7}, \quad \bar{m}_h = \bar{m}_{h0} m_h, \quad \bar{m}_{ss} = \bar{m}_{h0} m_{ss}, \quad \bar{h}_r = \bar{s}_{sT} h_r,$$
$$\bar{S}_s = \bar{s}_{sT} s_s, \quad \bar{h}_c = \bar{h}_{cT} h_c, \quad \bar{h}_b = \bar{h}_{cT} h_b, \quad \bar{g}_{pp} = \bar{h}_{cT} g_{pp},$$
$$\bar{f}_{pp} = \bar{h}_{cT} f_{pp}, \quad \bar{f}_{bpp} = \bar{h}_{cT} f_{bpp}, \quad \bar{s}_q = \bar{h}_{cT} s_q, \quad \bar{l} = \bar{h}_{cT} l, \quad \bar{c} = \bar{h}_{cT} c, \tag{33}$$

where $\bar{s}_{sT}$ and $\bar{h}_{cT}$ are the experimentally determined total concentrations of squalene synthase and HMG-CoA in a resting hepatocyte cell [5]. Substitut-

ing these rescalings into equations (20) through (32), we obtain

$$\frac{dm_h}{dt} = \frac{\mu_1}{1 + \left(\kappa_1(1 + (\frac{c}{\kappa_3})^{x_c})\right)^{x_h}} - \delta_1 m_h, \tag{34}$$

$$\frac{dm_{ss}}{dt} = \frac{\mu_2}{1 + \left(\kappa_2(1 + (\frac{c}{\kappa_3})^{x_c})\right)^{x_s}} - \delta_2 m_{ss}, \tag{35}$$

$$\frac{dh_r}{dt} = \mu_3 m_h + \kappa_{-4}\alpha h_b - \kappa_4 \alpha h_r h_c + \mu_5 \alpha h_b$$
$$- \delta_3 h_r \left(1 + \delta_{hg}\frac{g_{pp}}{g_{pp} + K_6} + \delta_{hf}\frac{f_{pp}}{f_{pp} + K_9} + \delta_{hl}\frac{l}{l + K_7} + \right.$$
$$\left. \delta_{hc}\frac{c}{c + K_8}\right), \tag{36}$$

$$\frac{ds_s}{dt} = \mu_4 m_{ss} + \kappa_{-5}\alpha f_{bpp} - \kappa_5 \alpha s_s f_{pp}^2 + \mu_7 \alpha f_{bpp} -$$
$$\delta_4 s_s \left(1 + \delta_{sc}\frac{c}{c + K_{10}}\right), \tag{37}$$

$$\frac{dh_c}{dt} = \kappa_{-4}h_b - \kappa_4 h_r h_c + \omega, \tag{38}$$

$$\frac{dh_b}{dt} = -\kappa_{-4}h_b + \kappa_4 h_r h_c - \mu_5 h_b - \delta_3 h_b, \tag{39}$$

$$\frac{dg_{pp}}{dt} = \mu_5 h_b - \delta_5 g_{pp} - \mu_6 g_{pp}, \tag{40}$$

$$\frac{df_{pp}}{dt} = \mu_6 g_{pp} - \delta_6 f_{pp} - 2\kappa_5 s_s f_{pp}^2 + 2\kappa_{-5}f_{bpp}, \tag{41}$$

$$\frac{df_{bpp}}{dt} = \kappa_5 s_s f_{bpp}^2 - \kappa_{-5}f_{bpp} - \mu_7 f_{bpp} - \delta_4 f_{bpp}, \tag{42}$$

$$\frac{ds_q}{dt} = \mu_7 f_{bpp} - \mu_8 s_q, \tag{43}$$

$$\frac{dl}{dt} = \mu_8 s_q - \delta_7 l - \mu_9 l, \tag{44}$$

$$\frac{dc}{dt} = \frac{\mu_9 l - \delta_8 c}{1 - x_c(s_0 s' + x_h g_{h0} s'_{bh} + x_s g_{ss0} s'_{bss})}, \tag{45}$$

11

with the non-dimensional initial conditions, at $t = 0$, given by

$$m_h(0) = 1, \quad m_{ss}(0) = 1, \quad h_r(0) = 0, \quad s_s(0) = 0, \quad h_c(0) = 0,$$
$$h_b(0) = 0, \quad g_{pp}(0) = 0, \quad f_{pp}(0) = 0, \quad f_{bpp}(0) = 0, \quad s_q(0) = 0,$$
$$l(0) = 0 \quad \text{and} \quad c(0) = 0, \tag{46}$$

and the non-dimensional parameters summarised in Table 2.

3.2. Model parameterisation

Wherever possible data from human liver (hepatocyte G2; HepG2) cells was used to inform our parameter values. Where values have been unavailable from HepG2 cells, other sources have included human liver microsomes (pieces of the endoplasmic reticulum used in some experimental work) or Chinese hamster ovary cells. Details regarding the estimation of all parameter values is provided in Appendix C, whilst Table 1 summarises each dimensional parameter, their value and source. Non-dimensional parameters are stated in Table 2.

In cases where no information was available, approximations were first made based on similar occuring reactions and processes, e.g. rates of mRNA degradation, as detailed in Appendix C. For instance, rates calculated from Bhattacharya et al. [2] regarding HMGCR and cholesterol synthesis, specifically binding affinities and degradation rates relating to HMGCR mRNA, HMGCR and cholesterol, were used to initially inform rates corresponding to squalene synthase synthesis and degradation as well as (non)sterol production rates. Using Matlab [21] the model was then simulated numerically (using the ode15s solver) and analysed via a local sensitivity analysis (coded directly into Matlab). The sensitivity analysis was used to ascertain the importance of the unknown assumed parameter values in affecting the total cholesterol concentration in an heptaocyte. Based on the findings of this analysis, parameter values were then adjusted accordingly (as detailed in Appendix C) to ensure the model reproduced previously determined cholesterol concentrations [2].

In the absence of any available data in other cell systems with which to compare any determined values, the additional effects of farnesyl-PP, geranyl-PP, lanosterol and cholesterol on HMGCR degradation and cholesterol on

12

that of squalene synthase degradation (δ_{hg}, δ_{hf}, δ_{hl}, δ_{hc}, δ_{sc}) were set equal to unity.

It is important to note that the utilisation of cholesterol and farnesyl-PP can vary depending on other intracellular processes. To simplify our model, we have assumed a constant value of cholesterol and farnesyl-PP degradation to include cellular utilisation, based on the work by Bhattacharya et al. [2].

Table 1: Dimensional parameters. Here "Param." denotes parameter, "molec" molecules, "SqS" squalene synthase.

Param.	Description	Value	Units	Reference
$\bar{m}_{h0}$	Initial HMGCR mRNA concentration.	3.0×10^9	molec./ml	[30]
$\bar{m}_{ss0}$	Initial SqS mRNA concentration.	3.0×10^9	molec./ml	[30]
$\bar{s}_{sT}$	Total SqS synthase concentration.	7.59×10^{14}	molec./ml	[5]
$\bar{h}_{cT}$	Total HMGCoA concentration.	1.98×10^{15}	molec./ml	[33, 38]
$\bar{s}_0$	Total SREBP-2 concentration.	8.21×10^{16}	molec./ml	[31, 2]
$\bar{g}_{h0}$	HMGCR gene concentration.	2.11×10^9	molec./ml	[41]/This study.
$\bar{g}_{ss0}$	SqS gene concentration.	2.11×10^9	molec./ml	This study.
$\bar{\mu}_1^*$	HMGCR transcription.	5.17×10^5	$\frac{\text{molec.}}{\text{ml.s}}$	[8, 12]
$\bar{\mu}_2^*$	SqS transcription.	4.65×10^5	$\frac{\text{molec.}}{\text{ml.s}}$	[8, 37]
$\bar{\mu}_3$	HMGCR translation	3.32×10^{-2}	1/s	[39, 17]
$\bar{\mu}_4$	SqS translation.	1.91×10^{-2}	1/s	[39, 36]
$\bar{\mu}_5$	Geranyl-PP formation.	4.33×10^{-2}	1/s	[15, 33, 43]
$\bar{\mu}_6$	Farnesyl-PP formation.	4.33×10^{-2}	1/s	[15, 33, 47]
$\bar{\mu}_7$	SqS formation.	2.17×10^{-1}	1/s	This study.
$\bar{\mu}_8$	Lanosterol formation.	4.33×10^{-2}	1/s	[15, 33, 47]
$\bar{\mu}_9$	Cholesterol formation.	4.33×10^{-2}	1/s	[15, 33, 47]
$\bar{K}_1$	SREBP-2-HMGCR gene binding affinity.	8.21×10^{12}	molec./ml	[29]/This study.
$\bar{K}_2$	SREBP-2-SqS gene binding affinity.	8.21×10^{12}	molec./ml	[29]/This study.
$\bar{K}_3$	Cholesterol-SREBP-2 disassociation constant.	1.49×10^{16}	molec./ml	[46]/This study.
$\bar{\kappa}_4$	HMGCR-HMGCoA association.	1.39×10^{-16}	$\frac{\text{ml}}{\text{molec.s}}$	This study.

13

Table 1 – continued

$\bar{\kappa}_{-4}$	HMGCR-HMGCoA disassociation.	1.75×10^{-7}	1/s	This study
$\bar{\kappa}_5$	SqS - Farnesyl-PP association.	1.76×10^{-30}	$\frac{\mathrm{ml}^2}{\mathrm{molec}^2.\mathrm{s}}$	This study
$\bar{\kappa}_{-5}$	SqS - Farnesyl-PP disassociation.	1.75×10^{-5}	1/s	This study.
$\bar{K}_6$	Michaelis-Menten constant for geranyl-PP/HMGCR degradation.	5.00×10^9	molec./ml	This study.
$\bar{K}_7$	Michaelis-Menten constant for lanosterol/HMGCR degradation.	5.00×10^{12}	molec./ml	This study.
$\bar{K}_8$	Michaelis-Menten constant for cholesterol/HMGCR degradation.	5.00×10^{17}	molec./ml	This study.
$\bar{K}_9$	Michaelis-Menten constant for farnesyl-PP/HMGCR degradation.	5.00×10^{11}	molec./ml	This study.
$\bar{K}_{10}$	Michaelis-Menten constant for cholesterol/SqS degradation.	5.00×10^{17}	molec./ml	This study.
$\bar{\delta}_1$	HMGCR mRNA degradation.	4.48×10^{-5}	1/s	[3]
$\bar{\delta}_2$	SqS mRNA degradation.	4.48×10^{-5}	1/s	This study.
$\bar{\delta}_3$	HMGCR degradation.	6.42×10^{-5}	1/s	[44]
$\bar{\delta}_4$	SqS degradation.	6.42×10^{-5}	1/s	This study.
$\bar{\delta}_5$	Geranyl-PP degradation.	1.20×10^{-4}	1/s	This study.
$\bar{\delta}_6$	Farnesyl-PP degradation.	1.20×10^{-4}	1/s	This study.
$\bar{\delta}_7$	Lanosterol degradation.	1.20×10^{-4}	1/s	This study.
$\bar{\delta}_8$	Cholesterol degradation.	1.20×10^{-4}	1/s	[2]
δ_{hg}	Additional effect of geranyl-PP on HMGCR degradation.	1	-	This study.
δ_{hf}	Additional effect of farnesyl-PP on HMGCR degradation.	1	-	This study.
δ_{hl}	Additional effect of lanosterol on HMGCR degradation.	1	-	This study.
δ_{hc}	Additional effect of cholesterol on HMGCR degradation.	1	-	This study.
δ_{sc}	Additional effect of cholesterol on SqS degradation.	1	-	This study.
$\bar{\omega}$	HMGCoA production.	3.90×10^{11}	molec./ml	This study.
x_h	Binding sites on HMGCR	3	-	[28]

14

Table 1 – continued

x_s	gene for SREBP-2. Binding sites on SqS gene for SREBP-2.	1	-	This study.
x_c	Molecules of cholesterol to inactivate SREBP-2.	4	-	[46, 16]

Table 2: Table of non-dimensional parameters, their relation to dimensional ones and value.

Parameter	Description	Definition	Value
s_0	Ratio of SREBP-2 to HMGCoA	$\bar{s}_0/\bar{h}_{cT}$	41.46
g_{h0}	Ratio of HMGCR gene to SREBP-2	$\bar{g}_{h0}/\bar{s}_0$	2.57×10^{-8}
g_{ss0}	Ratio of SqS gene to SREBP-2	$\bar{g}_{ss0}/\bar{s}_0$	2.57×10^{-8}
μ_1	HMGCR mRNA transcription.	$\frac{\bar{\mu}_1^*}{\bar{\delta}_7 \bar{m}_{h0}}$	1.44
μ_2	SqS mRNA transcription.	$\frac{\bar{\mu}_2^*}{\bar{\delta}_7 \bar{m}_{h0}}$	1.29
μ_3	HMGCR translation.	$\frac{\bar{\mu}_3 \bar{m}_{h0}}{\bar{\delta}_7 \bar{s}_{sT}}$	1.10×10^{-3}
μ_4	SqS translation.	$\frac{\bar{\mu}_4 \bar{m}_{h0}}{\bar{\delta}_7 \bar{s}_{sT}}$	6.29×10^{-4}
μ_5	Geranyl-PP production.	$\frac{\bar{\mu}_5}{\bar{\delta}_7}$	3.61×10^2
μ_6	Farnesyl-PP production.	$\frac{\bar{\mu}_6}{\bar{\delta}_7}$	3.61×10^2
μ_7	SqS production.	$\frac{\bar{\mu}_7}{\bar{\delta}_7}$	1.80×10^3
μ_8	Lanosterol production.	$\frac{\bar{\mu}_8}{\bar{\delta}_7}$	3.61×10^2
μ_9	Cholesterol production.	$\frac{\bar{\mu}_9}{\bar{\delta}_7}$	3.61×10^2
κ_1	SREBP-2-HMGCR gene binding affinity.	$\frac{\bar{K}_1}{\bar{s}_0}$	1×10^{-4}
κ_2	SREBP-2-SqS gene binding affinity.	$\frac{\bar{K}_2}{\bar{s}_0}$	1×10^{-4}
κ_3	Cholesterol-SREBP-2 dissociation constant.	$\frac{\bar{K}_3}{\bar{h}_{cT}}$	7.5
κ_4	HMGCR-HMGCoA association.	$\frac{\bar{\kappa}_4 \bar{s}_{sT}}{\bar{\delta}_7}$	8.83×10^2
κ_{-4}	HMGCR-HMGCoA disassociation.	$\frac{\bar{\kappa}_{-4}}{\bar{\delta}_7}$	1.46×10^{-3}
κ_5	SqS-farnesyl-PP association.	$\frac{\bar{\kappa}_5 \bar{h}_{cT} \bar{s}_{sT}}{\bar{\delta}_7}$	2.20×10^4
κ_{-5}	SqS-farnesyl-PP disassociation.	$\frac{\bar{\kappa}_{-5}}{\bar{\delta}_7}$	1.46×10^{-1}
K_6	Michaelis-Menten constant for geranyl-PP/HMGCR degradation.	$\frac{\bar{K}_6}{\bar{h}_{cT}}$	2.53×10^{-6}
K_7	Michaelis-Menten constant for lanosterol/HMGCR degradation.	$\frac{\bar{K}_7}{\bar{h}_{cT}}$	2.53×10^{-3}
K_8	Michaelis-Menten constant for cholesterol/HMGCR degradation.	$\frac{\bar{K}_8}{\bar{h}_{cT}}$	2.53×10^2
K_9	Michaelis-Menten constant	$\frac{\bar{K}_9}{\bar{h}_{cT}}$	2.53×10^{-4}

Table 2 – continued

K_{10}	for farnesyl-PP/HMGCR degradation. Michaelis-Menten constant for cholesterol/SqS degradation.	$\frac{\bar{K}_{10}}{\bar{h}_{cT}}$	2.53×10^2
δ_1	HMGCR mRNA degradation.	$\frac{\bar{\delta}_1}{\bar{\delta}_7}$	3.73×10^{-1}
δ_2	SqS mRNA degradation.	$\frac{\bar{\delta}_2}{\bar{\delta}_7}$	3.73×10^{-1}
δ_3	HMGCR degradation.	$\frac{\bar{\delta}_3}{\bar{\delta}_7}$	5.35×10^{-1}
δ_4	SqS degradation.	$\frac{\bar{\delta}_4}{\bar{\delta}_7}$	5.35×10^{-1}
δ_5	Geranyl-PP degradation.	$\frac{\bar{\delta}_5}{\bar{\delta}_7}$	1
δ_6	Farnesyl-PP degradation.	$\frac{\bar{\delta}_6}{\bar{\delta}_7}$	1
δ_7	Lanosterol degradation.	$\frac{\bar{\delta}_7}{\bar{\delta}_7}$	1
δ_8	Cholesterol degradation.	$\frac{\bar{\delta}_8}{\bar{\delta}_7}$	1
ω	HMGCoA production.	$\frac{\bar{\omega}}{\bar{\delta}_7 \bar{h}_{c0}}$	0.82
α	Ratio of total HMGCoA to SqS.	$\frac{\bar{h}_{cT}}{\bar{s}_{sT}}$	2.61

4. Analysis of numerical results

In this section we present numerical solutions to equations (34) to (46), parameterised by Table 2, obtained using the MATLAB stiff differential equation solver ode15s [21]. Results are shown in Figure 2. Time has been re-dimensionalised on the x-axis and simulations run until the system reaches steady-state.

Figure 2 shows the initial increase of HMGCR and squalene synthase mRNA; a result of no cholesterol being initially present in the system. HMGCR and squalene synthase mRNA transcription subsequently leads to their translation into their respective proteins. As HMGCR increases it binds to HMG-CoA leading to a subsequent decrease in its levels. This substrate-enzyme reaction leads to increases in geranyl-PP, farnesyl-PP, bound farnesyl-PP with squalene synthase, squalene, lanosterol and finally cholesterol. The observed decrease in each entity within the network at approximately 20 hours is the result of global and local feedbacks within the system. Firstly, the increase in cholesterol leads, via the negative feedback between cholesterol and SREBP-2 transcription of HMGCR mRNA and squalene synthase mRNA, to a decrease in the concentration of HMGCR and squalene synthase, respectively. This globally controlled feedback reduction in the two enzymes subsequently means less of the central cascade products are now being synthesised. This feedback is explored in more detail in Section 7.1. Simultaneously,
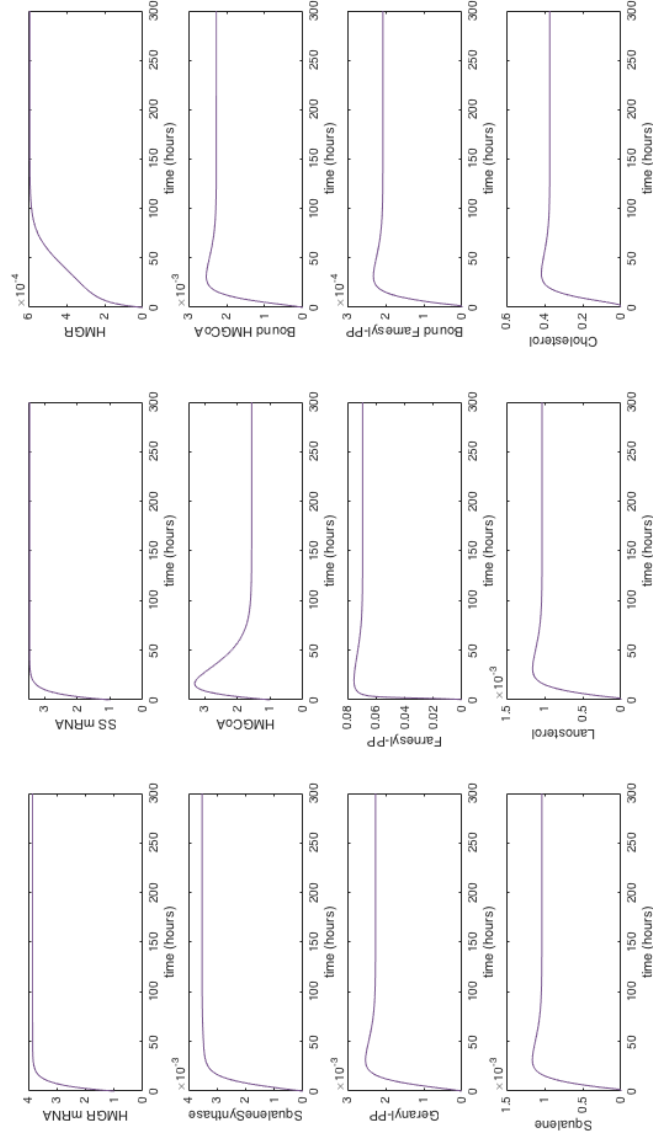
16

Figure 2: Numerical solutions to equations (34) to (46) with parameter values detailed in Table 2. Solutions show the response of HMGCR and squalene synthase mRNA to initial zero cholesterol concentrations, the subsequent increase in HMGCR and squalene synthase which allows the synthesis of cascade products geranyl-PP, farnesyl-PP, squalene, lanosterol and finally cholesterol.

17

and more locally, negative feedbacks from geranyl-PP, farnesyl-PP, lanosterol and cholesterol seek to limit the enzymatic action of HMGCR and squalene synthase by increasing their rates of degradation. These local feedbacks are explored in more detail in Section 9.

The subsequent decrease in cholesterol levels leads to a small increase in HMGCR and squalene synthase mRNA transcription. Eventually the solutions evolve to reach a steady-state. Solutions of the model show that concentrations of both farnesyl-PP and cholesterol are greater than those of other cascade products; geranyl-PP, squalene and lanosterol. One reason for this could be because farnesyl-PP is a major branch point in the pathway and is used (as is cholesterol) in a greater number of cell processes, thus their respective concentrations need to be higher. We note that HMGCoA initially increases (as a result of its own synthesis) before decreasing to steady-state levels due to increased HMGCR levels.

Direct comparison with experimental values for the concentration of each entity within the pathway is difficult given a lack of reported values in the literature. In the case of HMGCR mRNA we can approximate this via Rudling et al. [30] who states there are 30 copies of HMGCR mRNA found in each human liver cell under basal conditions. This leads to a concentration of 3.00×10^{10} molecules/ml, for which our result of 1.13×10^{10} molecules/ml is very similar. Our concentrations of HMGCR mRNA, HMGCR and cholesterol are also in agreement with those previously reported in Bhattacharya et al. [2].

5. Model Analysis

In this and subsequent sections we undertake a comprehensive analysis of the mevalonate pathway model. Given the overall network complexity and difficulty in obtaining analytical solutions to the system of governing equations we begin with a sensitivity analysis in Section 5.1. Results from this highlight enzyme-rate rate limiting steps within the pathway which are explored in more detail analytically in Section 6. We consider a simplified model of the pathway, containing the key enzyme-substrate reactions and feedbacks within the pathway in Section 7, in order to examine the steady-states of the system and their stability. Numerical experiments are conducted in Section 8 to verify our findings.

18

5.1. Sensitivity analysis

We conducted a local sensitivity analysis, varying each parameter in turn, up to 100-fold above and below the values reported in Table 2. We quantitatively measured, primarily, the effect of parameter variation on the steady-state cholesterol concentrations (in relation to the unperturbed system) whilst also looking for significant variations in key elements of the pathway, for example steady-state farnesyl-PP concentrations and differences in the dynamic behaviour of each model variable. Varying the model parameters up to 100-fold allows us to explore the robustness of the pathway to changes greater than those biologically feasible thereby ensuring all possible effects have been explored.

In what follows we present our results by discussing parameters related to specific processes within the pathway (e.g. HMGCR synthesis) wherever possible. Given their number and to ascertain their effects separately, negative feedbacks within the pathway are discussed separately in Sections 7.1 and 9. Not all parameters caused a notable change in the system; only those that did are discussed here.

The results of our local sensitivity analysis were subsequently confirmed by a metabolic control analysis in which the relationship between the system steady-states and the properties of the individual reactions was explored. The response coefficients were calculated via

$$\mathbf{R} = R_m^i = \frac{P_m}{S_i^{st}} \frac{\partial S_i^{st}}{\partial P_m},$$

where $\mathbf{R}$ is the matrix of response coefficients, P_m is each parameter value and S_i^{st} is the corresponding metabolite (mRNA/substrate/enzyme in our system) at steady-state.

5.1.1. HMGCoA synthesis (ω)

The HMGCoA-HMGCR reaction point in the pathway is the first rate limiting step in the cascade [34] and HMGCoA is the starting point of all the central cascade reactions. Hence decreasing HMGCoA availability 10-fold leads to an abundance of enzyme HMGCR (over 300% more) and leads to a reduction of over 90% in all cascade products except farnesyl-PP (73%).

Increasing the rate of HMGCoA synthesis 10-fold, decreases HMGCR concentrations by almost 100% due to the abundance of HMGCoA, but has only a moderate effect on the concentrations of cascade products (around 33%) including cholesterol. In all cases farnesyl-PP is more tightly regulated, and exhibits a smaller percentage change, than the rest of the cascade products. Thus the farnesyl-PP squalene synthase substrate-enzyme reaction appears to act as a second rate limiting step in the pathway, lending greater control to downstream cholesterol concentrations. This is explored in further detail in Section 6.

5.1.2. Genetic regulation of HMGCR (μ_1, μ_3, δ_1 and δ_3)

Parameter changes that induce an increase in HMGCR mRNA or HMGCR did not greatly affect the pathway. This is because the substrate HMGCoA is almost completely utilised and thus cholesterol increases are limited in spite of the amount of HMGCR being produced i.e. the binding of HMGCoA and HMGCR has reached its upper limit. This combined with the results of altering the rate of HMGCoA synthesis ω, show there is a careful balance of both enzyme HMGCR and substrate HMGCoA in order for cholesterol to be produced. If there is an abundance of either enzyme or substrate, the reaction will be limited by the lower of the two concentrations without a significant effect on cholesterol concentrations. However, biologically, we would always expect the concentration of enzyme to be less than the concentration of substrate.

On the other hand, decreasing the rates of transcription and translation (μ_1, μ_3) or increasing the rates of HMGCR mRNA and HMGCR degradation (δ_1 and δ_3) has a significant effect on cholesterol concentrations, as well as decreasing all the other cascade products. For example, decreasing the value of μ_1 or μ_3 by even one order of magnitude causes an 88% decrease in cholesterol levels. Increasing the value of δ_1 or δ_3 by one order of magnitude has a similar effect. Concentrations of HMGCR are, unsurprisingly, decreased leading to an accumulation of HMGCoA. Products of the central cascade are all decreased by around 88% (farnesyl-PP 68%). The reduction of cholesterol upregulates squalene synthase via the local squalene synthase degradation feedback shown in Figure 1.

20

5.2. Genetic regulation of squalene synthase (μ_2, μ_4, δ_2 and δ_4)

Parameter changes that cause an increase in squalene synthase mRNA or squalene synthase do not greatly affect the pathway. An abundance in squalene synthase leads to a significant decrease in farnesyl-PP, but the increase in cholesterol concentrations (as well as those of squalene and lanosterol) is only around 7%. Increasing the amount of squalene synthase does have a greater effect on cholesterol concentrations than increasing the amount of HMGCR, however we again see the balanace of enzyme and substrate limiting the reaction.

Parameter changes that cause a decrease in squalene synthase mRNA or squalene synthase have less of an effect on concentrations of cholesterol than a decrease in HMGCR. For example, decreasing the value of transcription of squalene synthase mRNA (μ_2) or translation of squalene (μ_4), by one order of magnitude causes a 39% decrease in cholesterol levels. Increasing the value of δ_2 (the degradation rate of squalene synthase mRNA) or δ_4 (the degradation rate of squalene synthase) by one order of magnitude has the same effect. In each case concentrations of squalene synthase are, unsurprisingly, decreased which leads to an accumulation of farnesyl-PP. Products downstream of the farnesyl-PP-squalene synthase reaction (bound farnesyl-PP, squalene, lanosterol and cholesterol) are all decreased by around 39%, another indicator of a limiting step at this point in the pathway. This decline in cholesterol and other cascade product concentrations slightly reduces HMGCR degradation (2% change) as expected. We can demonstrate the effect of the HMGCR degradation feedbacks by comparing the concentrations between one and two orders of magnitude change in δ_2 and δ_4, where cholesterol and lanosterol concentrations decrease by 92.6%, HMGCR concentrations increase by 8%.

5.2.1. Association and disassociation of HMGCR for HMGCoA and farnesyl-PP for squalene (κ_4, κ_{-4}, κ_5 and κ_{-5})

Altering the association rates of each of these enzyme and substrate reactions has a small effect on cholesterol levels and downstream cascade products. We found that decreasing the rate of binding (κ_5) in the squalene synthase-farnesyl-PP reaction, has a greater effect on cholesterol and downstream cascade product levels than decreasing the binding rate (κ_4) in the HMGCR-HMGCoA reaction, again indicating the importance of the squalene synthase-

farnesyl-PP rate limiting step. Altering the disassociation rates (κ_{-4} and κ_{-5}) of each reaction has no effect on cholesterol levels or indeed the rest of the system.

5.2.2. Production of geranyl-PP and squalene (μ_5 and μ_7)

Decreasing the rate at which either of the enzyme-substrate complexes are converted to a product decreases the concentrations of the respective downstream products. Specifically decreasing the rate of squalene production, has a lesser effect on products downstream of the reaction than decreasing the rate at which geranyl-PP is produced. Decreasing either of these rates leads to an increase in both substrate concentrations but, counter-intuitively, decreases the concentration of both enzymes. This happens for two reasons; firstly the enzymes are held in their bound rather than free forms (shown by an increase in bound substrate concentrations). Secondly, increases in each substrate concentration ensures that any enzyme synthesised or returned from disassociation with the enzyme-substrate complex is quickly bound by the excess substrate. Increasing the rate of complex to product conversion (μ_5 and μ_7) has very little effect on downstream cascade products, given they are limited by the amount of available substrate (HMGCoA and farnesyl-PP, respectively).

5.2.3. Production of farnesyl-PP and lanosterol (μ_6 and μ_8)

Increasing the production rate of farnesyl-PP and lanosterol has very little effect on the pathway and cholesterol levels. Interestingly, decreasing the production rate of farnesyl-PP has a greater effect on the central cascade products than decreasing the production of lanosterol. Decreasing μ_6 100-fold reduces cholesterol concentrations by 22%, reducing the degradation of HMGCR and squalene synthase, which increase by 1.5% and 3.4% respectively.

5.2.4. Production of cholesterol (μ_9)

Increasing the rate of production of cholesterol does not greatly affect cholesterol concentrations, however decreasing μ_9 has a small to moderate effect on cholesterol levels. However, the changes in lanosterol concentrations as a result, have the greatest effect on HMGCR concentrations via the local

22

degradation feedbacks, in comparison to parameter changes that induce an increase or reduction of geranyl-PP or farnesyl-PP - the other degradation feedbacks on HMGCR.

5.2.5. Degradation of farnesyl-PP (δ_6)

Decreasing the degradation rate of farnesyl-PP slightly increases the steady-state concentration of cholesterol and other downstream cascade products (within 10%). As expected this negatively effects both HMGCR and squalene synthase via the degradation feedbacks by a moderate amount in order to limit the increase in farnesyl-PP and cholesterol. However, increasing the degradation rate of farnesyl-PP by just one order of magnitude impacts the downstream cascade significantly, decreasing the concentrations of squalene, lanosterol and cholesterol by 52.4% (33.6% for farnesyl-PP). The decrease in cholesterol subsequently up-regulates HMGCR and squalene synthase levels. Interestingly, squalene synthase is increased slightly more than HMGCR. This could be to counteract the loss of farnesyl-PP through degradation, to ensure cholesterol concentrations are maintained.

5.2.6. Degradation of geranyl-PP and lanosterol (δ_5 and δ_7)

Altering the degradation rates of geranyl-PP and lanosterol have very little effect on the pathway or steady-state cholesterol levels. Increasing degradation of geranyl-PP by 100 fold moderately reduces the concentrations of the central cacade and slightly upregulates squalene synthase and HMGCR. Squalene synthase more so. Increasing the degradation rate of lanosterol by 100-fold also reduces the concentrations of lanosterol and cholesterol by approximately the same amount, however, HMGCR is upregulated more than squalene synthase. This is a result of the change in central cascade products and the role of the Michaelis-Menten responses affecting the feedbacks to HMGCR and squalene synthase, respectively.

5.2.7. Cholesterol degradation (δ_8)

Varying the rate of cholesterol degradation greatly effects cholesterol concentrations. As expected the increase in cholesterol concentrations downregulates HMGCR and squalene synthase via the local degradation feedbacks,

23

however only by around 1%. Similiarly for decreased cholesterol concentrations, HMGCR and squalene synthse are upregulated by around 0.1%.

5.2.8. Genetic binding affinities and stoichiometric coefficients (κ_1, κ_2, κ_3, x_c, x_h and x_s)

Binding affinities and stoichiometric coefficients involved with the genetic regulation of HMGCR and squalene synthase have very little effect on the system. Interestingly, reducing parameters involved in genetic regulation of HMGCR has a greater effect on the system than those in regulating squalene synthase, however these changes would indicate a fraction of a binding site which is biologically infeasible. Furthermore, decreasing the value of κ_3, the regulation of HMGCR and squalene synthase by cholesterol has the effect of decreasing cholesterol concentrations, significantly for a 100-fold decrease, whilst slightly upregulating HMGCR and squalene synthase.

5.2.9. Sensitivity analysis summary

Local sensitivity analysis has highlighted that a decrease in HMGCR (the first rate limiting step in the pathway), caused by parameters linked with its genetic regulation, significantly decreases steady-state cholesterol concentrations. However, increases in products linked with genetic regulation of HMGCR do not have a significant impact on steady-state cholesterol concentrations, due to the occurence of the second rate limiting step between squalene synthase and farnesyl-PP. The effect of decreasing products linked with genetic regulation of squalene synthase is not as significant as those linked with regulation of HMGCR.

An increase in products prior to the reaction of farnesyl-PP with squalene synthase rarely causes a significant change in cholesterol levels (the exception being a decrease in μ_5 reducing cholesterol concentrations significantly), whilst the degradation of farnesyl-PP has a high effect on downstream product concentrations. We found that, with the exception of decreasing μ_5, the rates of geranyl-PP and squalene formation, from the two enzyme-substrate reactions within the pathway, have a moderate effect on limiting downstream products formed in the pathway. In contrast, altering the rates of geranyl-PP and lanosterol degradation have little impact on the pathway. Cellular cholesterol concentrations are very sensitive to changes in the rate of choles-

24

terol esterification (degradation) without much interruption to the rest of the pathway.

Our results, as summarised in Table 3, demonstrate that the two rate limiting steps of HMGCR and HMGCoA and farnesyl-PP and squalene synthase, coupled with the negative feedback between cholesterol and SREBP-2, act as core regulators of products within the central cascade. The HMGCoA and HMGCR rate limiting step is aimed at controlling production of central cascade substrates, whilst that of farnesyl and squalene synthase appears two-fold; it acts to control the levels of lanosterol and ultimately cholesterol produced, but also regulate those of farnesyl-PP, given its role in other cell signalling pathways. Whilst the enzyme rate limiting step of HMGCR and HMGCoA follows one-to-one stoichometry, this differs for squalene synthase and farnesyl-PP; two molecules of farnesyl-PP reversibly bind to squalene synthase, to produce one molecule of complex bound farnesyl-PP. The effect of this is investigated further in Section 6.

Table 3: Sensitivity analysis summary. Results here indicate up to a 10% (denoted '+' or '-'), 10-50% ('++/- -'), greater than 50% ('+++/- - -') variation or no change ('NC') in the steady-state cholesterol levels for the parameterisation detailed in Table 1 for 10-fold parameter variations.
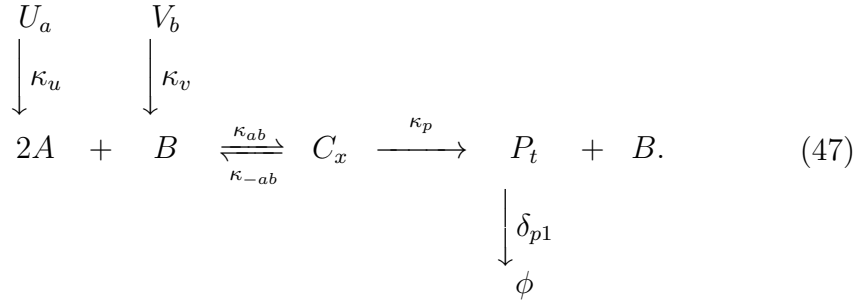
Change Made	Parameters Involved	Effect on Cholesterol
Increased HMGCoA	ω	++
Decreased HMGCoA	ω	—
Increased HMGCR	$\mu_1, \mu_3, \delta_1, \delta_3$	NC
Decreased HMGCR	$\mu_1, \mu_3, \delta_1, \delta_3$	- - -
Increased Squalene synthase	$\mu_2, \mu_4, \delta_2, \delta_4$	+
Decreased Squalene Synthase	$\mu_2, \mu_4, \delta_2, \delta_4$	- -
Increased Association of Enzymes	κ_4, κ_5	+
Decreased Association of Enzymes	κ_4, κ_5	- -
Dissociation of Enzymes	κ_{-4}, κ_{-5}	NC
Increased Product formation	μ_5, μ_7	NC
Decreased Product formation	μ_5	- - -
Decreased Product formation	μ_7	- -
Increased degrataion of FPP	δ_6	- - -
Decreased degradation of FPP	δ_6	+
Increased degradation	δ_5, δ_7	-
Decreased degradation	δ_5, δ_7	NC
Degradation of cholesterol	δ_8	+ + + / - - -
Stoichiometric coefficients	x_c, x_h, x_s	NC
Genetic binding affinities	K_1, K_2	NC
Increased genetic binding affinity	K_3	NC

25

Table 3 – continued

Decreased genetic binding affinity	K_3	-
Half Max degradation binding	K_6, K_7, K_8, K_9, K_10	NC
Increased Product formation	μ_6, μ_8	NC
Decreased Product formation	μ_6	-
Decreased Product formation	μ_8	NC
Increased Product formation	μ_9	NC
Decreased Product formation	μ_9	-

6. The farnesyl-PP - squalene synthase rate limiting step

Sensitivity analysis of the previous section has revealed evidence of two rate limiting steps working together to regulate homeostatic cholesterol levels. The first is that of the well documented HMGCR HMGCoA reaction, whilst the second involves farnesyl-PP reacting with squalene synthase. Here we investigate the role of the latter reaction, in particular the role of the stoichometry between farnesyl-PP and squalene synthase in effecting the creation of products downstream of this reaction. In order to do so we consider a simplified version of this part of the network as given by the reaction stated in equation (47).

$$
\begin{array}{ccccccc}
U_a & & V_b & & & & \\
\downarrow{\scriptstyle\kappa_u} & & \downarrow{\scriptstyle\kappa_v} & & & & \\
2A & + & B & \underset{\kappa_{-ab}}{\overset{\kappa_{ab}}{\rightleftharpoons}} & C_x & \xrightarrow{\kappa_p} & P_t \quad + \quad B. \\
& & & & & & \downarrow{\scriptstyle\delta_{p1}} \\
& & & & & & \phi
\end{array}
\tag{47}
$$

In this case we have employed A to represent farnesyl-PP, B squalene synthase, C_x the enzyme-substrate complex, P_t squalene and U_a and V_b the influx of substrate and enzyme respectively. For simplicity we assume a constant source of enzyme U_a and substrate V_b, at rates κ_u and κ_v, respectively, and we have removed the effect of the feedback of cholesterol onto squalene synthase degradation. Here κ_{ab} and κ_{-ab} represent the binding and unbinding, respectively, of A and B, κ_p is the rate at which the product is formed and finally

26

the degradation of P is represented by δ_{p1}. We observe that $A, B, C_x, P_t \geq 0$ is required for biologically feasible solutions.

Applying the law of mass action to equation (47) leads to

$$\frac{da}{dt} = -2a^2b\kappa_{ab} + 2c_x\kappa_{-ab} + u_a\kappa_u, \tag{48}$$

$$\frac{db}{dt} = -a^2b\kappa_{ab} + c_x\kappa_{-ab} + v_b\kappa_v + c_x\kappa_p, \tag{49}$$

$$\frac{dc_x}{dt} = a^2b\kappa_{ab} - c_x\kappa_{-ab} - c_x\kappa_p, \tag{50}$$

$$\frac{dp_t}{dt} = c_x\kappa_p - p_t\delta_{p1}, \tag{51}$$

with the initial conditions

$$a(0) = a_0, \qquad b(0) = b_0, \qquad c_x(0) = 0, \qquad p_t(0) = 0.$$

We observe that the addition of equations (49) and (50) leads to

$$\frac{da}{dt} + \frac{db}{dt} = v_b\kappa_v,$$

which for large time becomes

$$b + c_x \sim v_b\kappa_v t. \tag{52}$$

This suggests that a, b, c_x and subsequently p_t follow solutions of the form

$$a \sim a_0 t^\alpha, \qquad b \sim b_0 t^\beta, \qquad c_x \sim c_{x0}t^\gamma \quad \text{and} \quad p_t \sim p_{t0}t^\lambda. \tag{53}$$

Substitution of these solution approximations into equations (48)-(51) leads to

$$a \sim Kt^{-1/2}, \qquad b \sim v_b\kappa_p t, \qquad c_x \sim \frac{u_a\kappa_u}{2\kappa_p} \quad \text{and} \quad p_t \sim \frac{u_a\kappa_u}{2\delta_{p1}}. \tag{54}$$

for which we have the results $a \to 0$, $b \to \infty$ for finite c_x and p_t. This result demonstrates that the substrate farnesyl-PP tends to zero, squalene synthase grows unboundedly in time whilst the complex (bound farnesyl-PP) and product (squalene) remain bounded for any degree of influx.

27

From this analysis we can conclude that the rate limiting interaction of squalene synthase and farnesyl-PP would ensure product formation (squalene) is finite and bounded regardless of whether the substrate (farnesyl-PP) or enzyme (squalene synthase) concentrations are bounded. Furthermore, if the levels of squalene are bounded the subsequent products i.e. lanosterol and cholesterol will also be bounded. Thus the mechanism has the downstream effect of ensuring cholesterol levels do not become excessive and alleviates the likelihood of biosynthetic cytotoxicity.

7. Steady-state stability analysis

The recent work of Bhattacharya et al. [2] demonstrated that a nonlinear ODE model describing cholesterol biosynthesis via HMGCR mRNA transcription and subsequent HMGCR translation was monostable. The mevalonate pathway examined here is essentially an extension of that model which incorporates further pathway details between HMGCR and cholesterol synthesis. The increased complexity raises the question as to whether the system exhibits a single real stable steady-state. In this section we utilise a reduction of the full model derived in Section 3 to investigatve this.

7.1. Model reduction

Given the complexity of the governing equations of the full pathway model system (equations (34)-(45)) we begin by simplifying the full pathway (henceforth known as the full model) of Figure 1 by that shown in Figure 3. Here the core product forming and branching points in the pathway have been retained such that w represents SREBP-2, u HMGCR, v squalene synthase, x HMGCoA, y farnesyl-PP and z cholesterol. Here x is produced at a rate A and the negative feedbacks between each relevant component have been included. We further assume that the cholesterol-SREBP-2 negative feedback is the fastest acting process in this reduced network, followed by the synthesis of HMGCR and squalene synthase, which occurs an order of magnitude slower. Subsequently the formation of x, y and z are assumed to be the slowest in the pathway. Finally, x, y and z decay proportional to their respective concentrations.
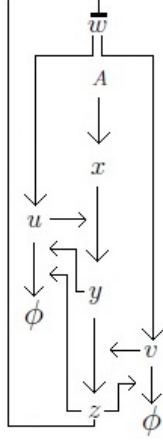
Figure 3: A model reduction of the mevalonate pathway which incorporates the key enzyme and substrate synthesis processes and branch points, along with their respective feedbacks. Here w represents SREBP-2, u HMGCR, v squalene synthase, x HMGCoA, y farnesyl-PP and z cholesterol, where x is produced at a rate A. It is assumed, as with the full-pathway model, that x, y and z decay proportional to their respective concentrations (not shown here).

Applying these assumptions and the law of mass action to the reduced pathway of Figure 3 leads to the following non-dimensional system of equations

$$\dot{x} = A - \mu_{r1}xu - \delta_{r1}x, \tag{55}$$

$$\dot{y} = \mu_{r1}\beta_x xu - \mu_{r2}yv - \delta_{r2}y, \tag{56}$$

$$\dot{z} = \mu_{r2}\beta_y yv - \delta_{r3}z, \tag{57}$$

$$\epsilon\dot{u} = \mu_{r3}w - \delta_{r4}u\left(\delta_{uz}\frac{z}{\kappa_{r1}+z} + \delta_{uy}\frac{y}{\kappa_{r2}+y} + 1\right), \tag{58}$$

$$\epsilon\dot{v} = \mu_{r4}w - \delta_{r5}v\left(\delta_{vz}\frac{z}{\kappa_{r3}+z} + 1\right), \tag{59}$$

$$\epsilon^2\dot{w} = \frac{\alpha_{r1}}{\kappa_{r4}+z^{n_1}} - \delta_{r6}w, \tag{60}$$

with the initial conditions

$$x = 1, \quad y = 1, \quad z = 1, \quad u = 1, \quad v = 1 \quad \text{and} \quad w = 1. \tag{61}$$

Here ϵ represents a small parameter and the remaining model parameters are given by μ_{r1} which represents the rate at which x produces y, μ_{r2} is the rate at which y produces z, μ_{r3} the rate at which u is transcribed, μ_{r4} the rate

29

at which v is transcribed, β_x and β_y are non-dimensional ratios representing the initial dimensional concentrations of x and y, and y and z, respectively and α_{r1} that rate at which w is produced. The effective binding sites of cholesterol on SREBP-2 is represented by n_1 and $\delta_{r1,2,3,4,5,6}$ represent the rate of degradation of x, y, z, u, v and w, respectively. Finally, $\kappa_{r1,2,3,4}$ are the Michaelis-Menten constants associated with the feedback of z on the rate of u degradation, y on that of u degradation, z on v degradation and z on w inhibition, respectively and δ_{uz}, δ_{uy} and δ_{vz} are dimensionless constants respectively representing their effect. As with the full model of Section 3 and for the sake of simplicity we henceforth assume, unless otherwise stated, $\delta_{uz} = 1 = \delta_{uy} = \delta_{vz}$.

Taking the $O(1)$ expansion of equations (55)-(60) leads to

$$\dot{x} = A - \frac{\tilde{\mu}_{r1}x}{(\kappa_{r4} + z^{n_1})\left(\frac{z}{\kappa_{r1}+z} + \frac{y}{\kappa_{r2}+y} + 1\right)} - \delta_{r1}x, \tag{62}$$

$$\dot{y} = \frac{\tilde{\mu}_{r1}\beta_x x}{(\kappa_{r4} + z^{n_1})\left(\frac{z}{\kappa_{r1}+z} + \frac{y}{\kappa_{r2}+y} + 1\right)} - \frac{\tilde{\mu}_{r2}y}{(\kappa_{r4} + z^{n_1})\left(\frac{z}{\kappa_{r3}+z} + 1\right)}$$
$$- \delta_{r2}y, \tag{63}$$

$$\dot{z} = \frac{\tilde{\mu}_{r2}\beta_y y}{(\kappa_{r4} + z^{n_1})\left(\frac{z}{\kappa_{r3}+z} + 1\right)} - \delta_{r3}z, \tag{64}$$

where

$$\tilde{\mu}_{r1} = \frac{\mu_{r1}\mu_{r3}\alpha_{r1}}{\delta_{r4}\delta_{r6}} \quad \text{and} \quad \tilde{\mu}_{r2} = \frac{\mu_{r2}\mu_{r4}\alpha_{r1}}{\delta_{r5}\delta_{r6}}. \tag{65}$$

Assuming the concentrations of cholesterol and farnesyl-PP are in excess and the rates of affinity of cholesterol for HMGCR and squalene synthase (k_{r1} and k_{r3}) and farnesyl-PP for HMGCR are significantly high such that $k_{r1}, k_{r3} \ll z$ and $k_{r2} \ll y$ leads to $k_{r1} + z \sim z$, $k_{r2} + y \sim y$ and $k_{r3} + z \sim z$. Thus

$$\dot{x} = A - \frac{\mu_{rr1}x}{\kappa_{r4} + z^{n_1}} - \delta_{r1}x = f(x,y,z), \tag{66}$$

$$\dot{y} = \frac{\mu_{rr1}\beta_x x}{\kappa_{r4} + z^{n_1}} - \frac{\mu_{rr2}y}{\kappa_{r4} + z^{n_1}} - \delta_{r2}y = g(x,y,z), \tag{67}$$

$$\dot{z} = \frac{\mu_{rr2}\beta_y y}{\kappa_{r4} + z^{n_1}} - \delta_{r3}z = h(x,y,z), \tag{68}$$

where $\mu_{rr1} = \frac{1}{3}\tilde{\mu}_{r1}$ and $\mu_{rr2} = \frac{1}{2}\tilde{\mu}_{r2}$.

7.2. Steady-state stability

Solving for the steady-states (x^*, y^*, z^*) of equations (66)-(68) leads to the polynomial (recalling that n_1 is an integer)

$$
\begin{aligned}
z^{2n_1+1}(\delta_{r1}\delta_{r2}\delta_{r3}) + z^{n_1+1}(\delta_{r1}\delta_{r3}\mu_{rr2} + 2\delta_{r1}\delta_{r2}\delta_{r3}\kappa_{r4} + \delta_{r2}\delta_{r3}\mu_{rr1}) \\
+ z(\delta_{r2}\delta_{r3}\mu_{rr1}\kappa_{r4} + \delta_{r1}\delta_{r2}\delta_{r3}\kappa_{r4}^2 + \delta_{r1}\delta_{r3}\mu_{rr2}\kappa_{r4} + \delta_{r3}\mu_{rr1}\mu_{rr2}) - \\
A\mu_{rr1}\mu_{rr2}\beta_x\beta_y = 0, \quad (69)
\end{aligned}
$$

569 which via Descartes' rule of signs [27] has only one positive root z^*. From
570 (66) and (67) it follows that the corresponding x^* and y^* are also positive.

571 Now the Jacobian of equations (66)-(68) is given by

$$
J = \begin{pmatrix}
\frac{-\mu_{rr1}}{\kappa_{r4}+z^{n_1}} - \delta_{r1} & 0 & \frac{n_1\mu_{rr1}xz^{n_1-1}}{(\kappa_{r4}+z^{n_1})^2} \\[2ex]
\frac{\mu_{rr1}\beta_x}{\kappa_{r4}+z^{n_1}} & \frac{-\mu_{rr2}}{\kappa_{r4}+z^{n_1}} - \delta_{r2} & \frac{-n_1\mu_{rr1}\beta_x xz^{n_1-1}}{(\kappa_{r4}+z^{n_1})^2} + \frac{n_1\mu_{rr2}yz^{n_1-1}}{(\kappa_{r4}+z^{n_1})^2} \\[2ex]
0 & \frac{\mu_{rr2}\beta_y}{\kappa_{r4}+z^{n_1}} & \frac{-n_1\mu_{rr2}\beta_y yz^{n_1-1}}{(\kappa_{r4}+z^{n_1})^2} - \delta_{r3}
\end{pmatrix},
$$

572 which allows us to determine the characteristic equation

$$
\lambda^3 + a_1\lambda^2 + a_2\lambda + a_3 = 0,
$$

573 where

$$
\begin{aligned}
a_1 = -(f_x + g_y + h_z), \qquad a_2 = f_x(g_y + h_z) + g_yh_z - g_zh_y \\
\text{and} \qquad a_3 = -(f_x(g_yh_z - g_zh_y) + f_zg_xh_y). \quad (70)
\end{aligned}
$$

574 Now for (x^*, y^*, z^*) to be stable we require $Re(\lambda) < 0$ meaning that the
575 following Routh–Hurwitz conditions [27] must hold

$$
a_1 > 0, \quad a_3 > 0 \quad \text{and} \quad a_1a_2 - a_3 > 0. \quad (71)
$$

576 It is easily seen that $f_x, g_y, h_z < 0$ (diagonal entries of J) whilst $f_z, g_x, h_y > 0$.
577 The remaining non-zero term of the Jacobian is

$$
g_z = -\left(\frac{n_1 z^{n_1-1}}{\kappa_{r4} + z^{n_1}}\right)\left(\frac{\mu_{rr1}\beta_x x}{\kappa_{r4} + z^{n_1}} - \frac{\mu_{rr2}y}{\kappa_{r4} + z^{n_1}}\right).
$$

31

578 Both sets of brackets are clearly positive at steady–state (the second set from
579 (67)) and so we have $g_z < 0$ at the steady–state.

580 Using the signs of the Jacobian entries at steady state immediately gives
581 $a_1 > 0$ and, with a little work we can readily use them to deduce that
582 $a_1 a_2 - a_3 > 0$. In order to show the remaining required inequality we cannot
583 use the signs of the Jacobian entries alone. Instead we first simplify notation
584 by writing

$$\alpha_1 = \frac{-\mu_{rr1}}{\kappa_{r4} + z^{n_1}}, \qquad \alpha_2 = \frac{-\mu_{rr2}}{\kappa_{r4} + z^{n_1}},$$

$$\gamma_1 = \frac{n_1 \mu_{rr1} x z^{n_1-1}}{(\kappa_{r4} + z^{n_1})^2}, \qquad \gamma_2 = \frac{n_1 \mu_{rr2} y z^{n_1-1}}{(\kappa_{r4} + z^{n_1})^2},$$

585 noting that each of these is non-negative. The Jacobian can then be written
586 as

$$J = \begin{pmatrix} -\alpha_1 - \delta_{r1} & 0 & \gamma_1 \\ \alpha_1 \beta_x & -\alpha_2 - \delta_{r2} & -\gamma_1 \beta_x + \gamma_2 \\ 0 & \alpha_2 \beta_y & -\gamma_2 \beta_y - \delta_{r3} \end{pmatrix},$$

587 and a_3 as

$$\begin{aligned} a_3 &= (\alpha_1 + \delta_{r1})\left((\alpha_2 + \delta_{r2})(\gamma_2 \beta_y + \delta_{r3}) + \alpha_2 \beta_y (\gamma_1 \beta_x (\gamma_1 \beta_x - \gamma_2))\right) \\ &\quad - \gamma_1 \alpha_1 \beta_x \alpha_2 \beta_y \\ &= (\alpha_1 + \delta_{r1})\left(\alpha_2 \delta_{r3} + \gamma_2 \beta_y \delta_{r2} + \delta_{r2} \delta_{r3}\right) + \delta_{r1} \alpha_2 \gamma_1 \beta_x \beta_y. \end{aligned}$$

588 Since each symbol is non-negative we immediately have that $a_3 > 0$ as re-
589 quired. Thus (x^*, y^*, z^*) is stable.

590 In order to provide a check of the stability obtained from the reduced model,
591 we numerically calculated the Jacobian for the full model system using the
592 parameter values detailed in Table 2. All eigenvalues are found to be negative
593 or approximately zero, for a range of initial conditions.

8. Periodic solutions

595 The results of Section 7 have demonstrated that the mevalonate pathway
596 exhibits one real steady-state. Both this model and that of Bhattacharya et

32

al. [2] include the negative regulation of SREBP-2 by cholesterol. In the case of the three variable model analysed by Bhattacharya and colleagues, they demonstrated that the system could exhibit periodic behaviour under certain model parameterisations. As such we now investigate numerically whether it is possible for the mevalonate pathway model to exhibit oscillatory solutions.

Our investigations focused on the parameters κ_1, κ_3, x_c and δ_8 given they are directly involved in the cholesterol-SREBP-2 feedback, are parameters for which periodic behaviour was shown in [2], and the results of varying all other model parameters in Section 5.1 produced no periodic behaviour.

Local sensitivity analysis of κ_1, κ_2, κ_3, x_c and δ_8 revealed the presence of periodic (damped or undamped) behaviour within the system, an example of which is shown in Figure 4. The presence of oscillatory behaviour for other parameter values showed comparable results. We note the increase in concentration of HMGCoA in Figure 4 is a result of the choice in w made to demonstrate the existence of oscillatory solutions. We sought to numerically investigate further the likelihood of a Hopf bifurication within the mevalonate pathway, as a result of this feedback, and undertook a phase space analysis using MATLAB'S ode15s solver and the plot3 function. We found that the system exhibits an unstable fixed point surrounded by a stable limit cycle and thus appears to undergo a supercritical Hopf bifurcation (results not shown). This was found to be the case when considering the HMGCR mRNA, HMGCR and cholesterol phase space as well as that for squalene synthase mRNA, squalene and cholesterol.

These results indicate that the full mevalonate pathway model is able to produce periodic behaviour, similar to that related to more simplified networks within it (e.g. HMGCR mRNA, HMGCR and cholesterol), so long as the global scale negative feedback between cholesterol and SREBP-2 is present.

9. Investigating feedbacks

In this section we consider how feedbacks within the mevalonate pathway contribute to the robust control of cholesterol concentrations. Whilst in previous sections we have focused on the role of the global cholesterol-SREBP-2 negative feedback, here we consider the effect of geranyl-PP, farnesyl-PP, lanosterol and cholesterol regulating the degradation of HMGCR, and cholesterol regulating the degradation of squalene synthase, respectively.
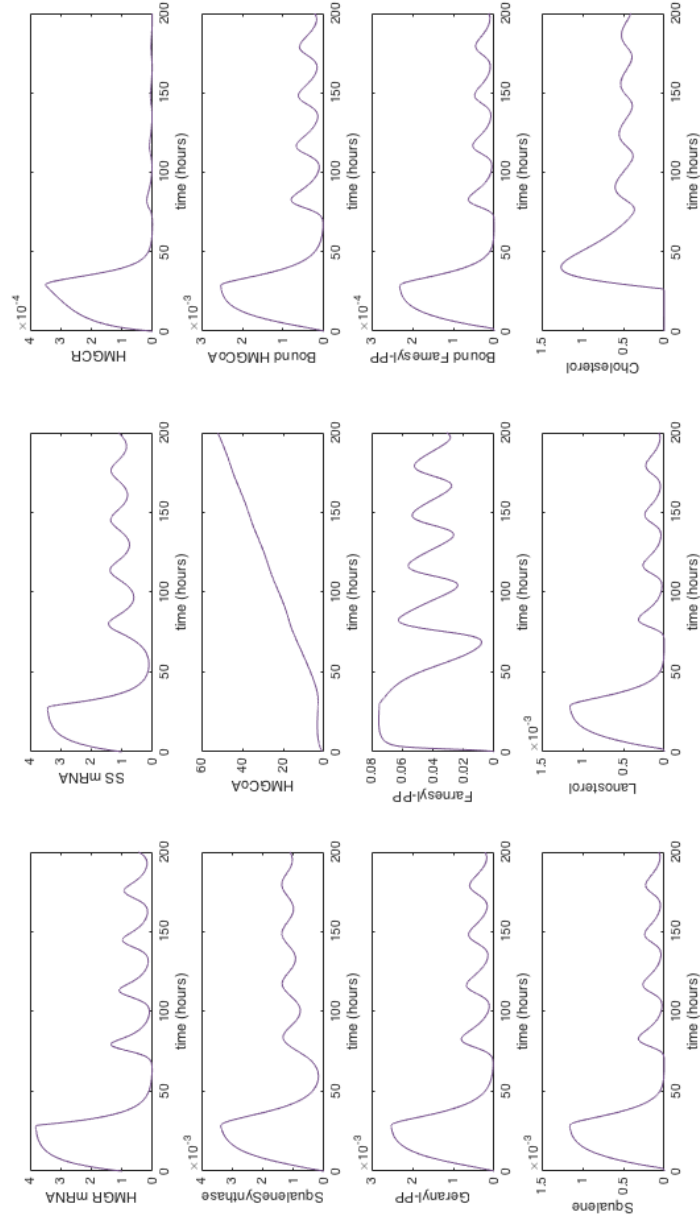
Figure 4: Solutions to the system of equations (34) to (46) for which periodic behaviour is exhibited. In this case $\kappa_1 = 1 \times 10^{-12}$, $\kappa_2 = 1 \times 10^{-12}$, $\kappa_3 = 3.74 \times 10^{-4}$, $\delta_8 = 0.1$, with all other parameters as in Table 2.

34

Given the complexity of the full pathway we began by considering the reduced model shown in Figure 3. This allowed for initial examination of the effect of the feedbacks on the core elements of the network (e.g. rate limiting steps and core products), rather than each individual entity in the full pathway. We identified each feedback in Figure 3 as: (1) $z \to u$ (cholesterol to HMGCR); (2) $y \to u$ (farnesyl-PP to HMGCR); and (3) $z \to v$ (cholesterol to squalene synthase).

We undertook numerical simulations of equations (55) - (60) using the MAT-LAB solver ode15s, assuming $\epsilon = 0.1$ under the eight scenarios detailed in Table 4; when all feedbacks were present, no feedbacks were present, each feedback acted independently and pair-wise. We recorded the difference in steady-state cholesterol concentration, measured as a percentage relative to when all feedbacks were present, in Table 4.

The results in Table 4 clearly show that for fewer feedbacks steady-state cholesterol concentrations increase. When no feedbacks are present, cholesterol levels increase by 27.4% in comparison to when all feedbacks are present. Individually, the feedback from farnesyl-PP onto HMGCR has the greatest effect on regulating cholesterol levels, whereas those from cholesterol to HMGCR and squalene synthase have the least similar effect. Interestingly our results demonstrate that the feedbacks between cholesterol and HMGCR and squalene synthase, respectively, together have just as tight a control on cholesterol as that of the feedback from farnesyl-PP to HMGCR. The results of Table 4 also show that local positive feedbacks affecting the rates of HMGCR and squalene synthase degradation act together with the two rate limiting steps in which they are respectively involved, to tightly regulate the concentration of cholesterol. Importantly, they are able to do so more directly and thus more rapidly, given less regulatory steps are involved, than via the feedback between cholesterol and SREBP-2.

To test the robustness of the feedback responses, specifically the transient concentration of cholesterol, we introduced a transient influx of cholesterol, B in to z such that

$$B = \begin{cases} 1, & \text{for } 0.10 \le t \le 0.15, \\ 0 & \text{otherwise.} \end{cases} \tag{72}$$

under differing feedback scenarios.

Table 4: The percentage relative difference in steady-state cholesterol concentration for when different feedbacks are included compared to when all three feedbacks are in play for the reduced model of Figure 3. In the case of comparing feedbacks either individually or pairwise, the other feedbacks were turned off. Here: (1) $z \to u$ (cholesterol to HMGCR); (2) $y \to u$ (intermediate substrates to HMGCR); and (3) $z \to v$ (cholesterol to squalene synthase) as, defined in Figure 3.

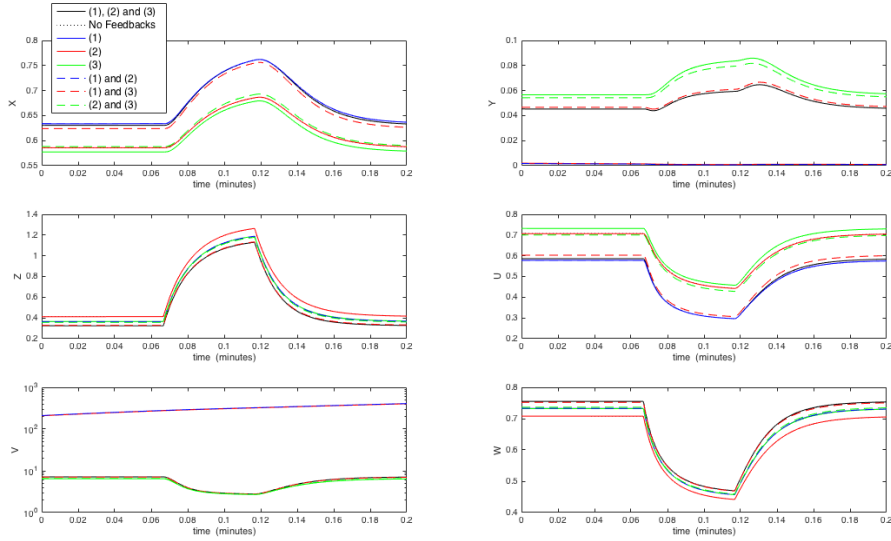| Scenario	Corresponding weighting parameters	Percentage increase in steady-state cholesterol levels.
No feedbacks	$\delta_{uz} = 0 = \delta_{uy} = \delta_{vz}$.	27.4%
(1)	$\delta_{uz} = 1, \delta_{uy} = 0 = \delta_{vz}$.	12.6%
(2)	$\delta_{uz} = 0, \delta_{uy} = 1, \delta_{vz} = 0$.	1.6%
(3)	$\delta_{uz} = 0 = \delta_{uy}, \delta_{vz} = 1$.	12.9%
(1), (2)	$\delta_{uz} = 1 = \delta_{uy}, \delta_{vz} = 0$.	12.6%
(1), (3)	$\delta_{uz} = 1, \delta_{uy} = 0, \delta_{vz} = 1$.	1.6%
(2), (3)	$\delta_{uz} = 0, \delta_{uy} = 1 = \delta_{vz}$.	10.3%

Figure 5: The impact of feedbacks on the reduced model of Figure 3 for the case where z (cholesterol) is increased for $0.10 < t < 0.15$. Equations (55)-(60) were solved for all parameter set equal to one with the exception of $\epsilon = 0.1$. Solutions were allowed to reach steady-state before the effect of turning each feedback off was investigated.

Figure 5 demonstrates that each of the feedbacks tightly regulate the concentrations of x, y and z and that varying combinations of them did not alter the overall transient behaviour. Additionally in scenarios where feedback (3) was turned off, levels of y (farnesyl-PP) were very low as more squalene synthase is available to bind with farnesyl-PP to form squalene. This coupled with the analysis undertaken in Section 6 showing if the concentration of squalene synthase grows unbounded the rate limiting step between it and farnesyl-PP acts to control the downstream concentrations of lanosterol and subsequently cholesterol, demonstrates these two processes act together locally to tightly regulate cholesterol levels in this section of the pathway.

We undertook the same analysis of each feedback on the full model of the pathway, equations (34) to (46). We inhibited the feedbacks from: (1) cholesterol to HMGCR degradation; (2) farnesyl-PP to HMGCR degradation; and (3) cholesterol to squalene synthase degradation. We again conducted the same eight scenarios detailed in Table 4 and found all scenarios show the same transient behaviour in good agreement with the reduced model. The only notable change was were switching feedback (2) off led to slightly higher levels of HMGCR. This difference was not seen when feedback (3) was switched on concurrently to feedback (2).

10. CYP51 inhibition

So far we have demonstrated that cholesterol biosynthesis via the mevalonate pathway is a tightly regulated process; a result of two enzymatic rate limiting steps coupled with local and global feedbacks within the signalling network. In this section we show how these elements integrate together to ensure a robust network response to the effect of the fungicide agent CYP51. CYP51 is known to inhibit post lanosterol production processes and is used in crop protection as an anti-fungal agent. It acts by reducing cholesterol concentrations within the cell, thereby compromising cell wall integrity, ultimately leading to cell death. Concerns exist that this inhibition is likely to lead to increases in farnesyl-PP levels, thereby inducing unwanted side-effects within other cell signalling cascades who share cross-talk with farnesyl-PP.

To investigate the effect of CYP51 inhibition on the pathway we first ran the system of equations (34) to (46) to steady-state. Taking this as our starting
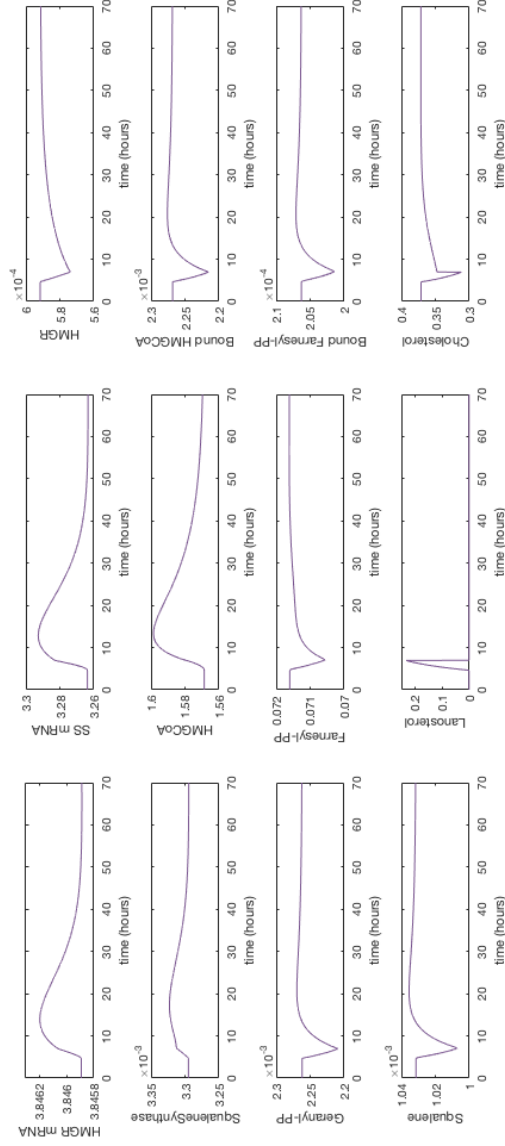
Figure 6: The effect of CYP51 inhibition on equations (34) to (46). Here $\mu_9 = 0$ at $\bar{t} = 5$ hours for 2 hours with $\kappa_3 = 0.075$, to simulate CYP51 inhibition as described by equation (73). Cholesterol concentrations decline which leads to a decrease in HMGCR levels as a result of the feedback between cholesterol and SREBP-2. Hence concentrations of geranyl-PP, farnesyl-PP and squalene all decline. All concentrations return to steady-state after CYP51 inhibition stops.

38

point we then simulated the effect of CYP51 inhibitors by letting

$$\mu_9 = \begin{cases} 0, & \text{for } 5 \le t \le 7, \\ 3.61 \times 10^2 & \text{otherwise.} \end{cases} \tag{73}$$

Results are shown in Figure 6. We see that CYP51 inhibition leads to a sharp increase in lanosterol and decline in cholesterol concentrations. Here we would expect an increase in HMGCR concentrations due to the rise in HMGCR mRNA, however the sharp increase in lanosterol concentration causes the degradation of HMGCR to be up-regulated, and so its concentration subsequently declines. The reduction in HMGCR thus leads to a decline in the central cascade products of geranyl-PP, farnesyl-PP and squalene. As a result we see that the change in these central cascade products is limited and that faresyl-PP levels actually reduce when production of cholesterol from lanosterol is inhibited. We note that an increase in inhibition of SREBP-2 by cholesterol ($\kappa_3 = 0.075$) was required in order to observe a response in HMGCR mRNA and squalene synthase mRNA.

11. Summary and conclusions

We have formulated, parameterised and analysed a nonlinear ODE model of the mevalonate cholesterol biosynthesis pathway. Our results show that the pathway tightly regulates steady-state and transient cholesterol levels via two rate limiting steps, internal local positive feedbacks affecting the rate of degradation of certain products within the pathway and a global negative feedback between cholesterol and SREBP-2.

A local sensitivity analysis of the model revealed a number of important regulatory points within the pathway. It highlighted that decreases in HMGCR levels has the greatest impact on downstream cholesterol levels either via variation in transcription or translation rates or the rate of HMGCR mRNA or HMGCR degradation. Increasing products prior to farnesyl-PP interacting with squalene synthase has a more significant effect on cholesterol levels in contrast to those after the reaction, the rates at which geranyl-PP and squalene are formed have the most significant effect. Altering the rate of cholesterol esterification has a significant impact on HMGCR and squalene synthase levels via the cholesterol SREBP-2 negative feedback loop.

Our sensitivity analysis also revealed the importance of the rate limiting enzyme substrate reactions of HMGCoA with HMGCR and farnesyl-PP with squalene synthase, the latter augmented by separate analytical analysis of the farnesyl-PP squalene synthase rate limiting step. The HMGCR-HMGCoA reaction was found to be an important upstream regulator of all main pathway products. That of farnesyl-PP and squalene synthase was found to be important in not only regulating downstream production of squalene, lanosterol and thus cholesterol, but in ensuring their levels did not increase significantly if levels of farnesyl-PP and squalene synthase did.

Analysis of a reduced model of the full pathway, which captured the main products and interactions between them, demonstrated that the system exhibits one real stable steady-state. The global feedback between cholesterol and SREBP-2 leads to monotonic, oscillatory and damped oscillatory behaviour, which agrees with the simplified HMGCR cholesterol regulatory model of [2]. This result shows that the feedback between cholesterol and SREBP-2 acts to globally regulate the dynamic pathway behaviour. This is in contrast to internal positive feedbacks between geranyl-PP, farnesylPP, lanosterol and the degradation of HMGCR and squalene synthase which our analysis demonstrated act directly within the pathway to tightly regulate overall cholesterol concentrations.

It is clear that feedbacks in the pathway act to control the dynamical response, enzyme concentrations and hence the concentration of cholesterol. The cholesterol-SREBP-2 feedback allows for cholesterol regulation of its own production over a longer timescale than those from geranyl-PP, farnesyl-PP, lanosterol and cholesterol to HMGCR and cholesterol to squalene synthase; which respond directly within the pathway to any variation in cholesterol levels. These direct responses alleviate the effect of further reactions in delaying the reduction of the entity they are targeting in the pathway.

Further evidence of the system's robust network control via the integration of two rate limiting steps and feedbacks was shown in the case of CYP51 inhibition. Simulations of CYP51 inhibition show the network response prevents cytotoxic build up of central cascade products geranyl-PP, squalene and farnesyl-PP. This is important since increased farnesyl-PP levels are linked with several other signalling pathways and excessive amounts are thought to cause tumours. In this way we have shown that CYP51 inhibitors would have little effect on farnesyl-PP concentrations in the mevalonate pathway.
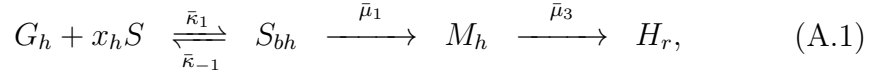
Given the importance of cholesterol synthesis in maintaining the integrity of cell function for many cellular phenotypes, the results of the work here are in many ways unsurprising. Cholesterol levels need to be tightly regulated, both in response to internal cellular variations and external factors, e.g. disease or dietary factors. Our work here has clearly demonstrated that the pathway is robustly designed and includes a number of 'fail safe' type mechanisms in the form of regulatory feedbacks and rate limiting steps which act in concert to provide a robust regulatory system. These results are in agreement with the work of August et al. [1] and Morgan et al. [25], who both demonstrated that the cholesterol biosynthesis aspects of their models were robust to parameter variation. The design of the network ensures that the integrity of cholesterol levels is not greatly compromised, should one or more of these mechanisms fail, thus ensuring cell survival is maintained.

Acknowledgement
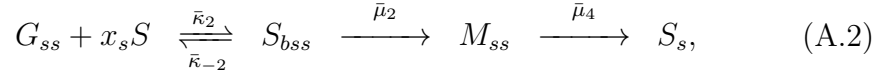
Appendix A. Biochemical reaction details

In order to formulate a mathematical model of the interactions shown in Figure 1 we first consider the biochemical details of each reaction. The binding of SREBP-2 to HMGCR DNA and subsequent mRNA and protein formation is governed by

$$
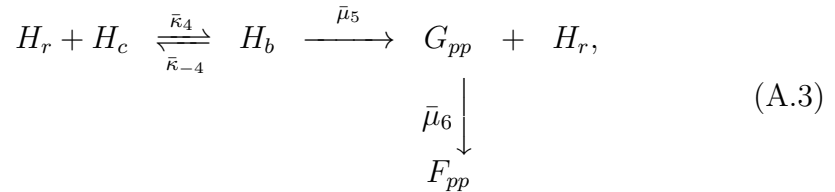G_h + x_h S \;\; \underset{\bar{\kappa}_{-1}}{\overset{\bar{\kappa}_1}{\rightleftharpoons}} \;\; S_{bh} \;\; \overset{\bar{\mu}_1}{\longrightarrow} \;\; M_h \;\; \overset{\bar{\mu}_3}{\longrightarrow} \;\; H_r, \qquad (A.1)
$$

where HMGCR free DNA is represented by G_h, S is SREBP-2, S_{bh} is SREBP-2 bound to the DNA, M_h is HMGCR mRNA and H_r is HMGCR. The constant reaction rates $\bar{\kappa}_1$ and $\bar{\kappa}_{-1}$ represent the binding and unbinding of SREBP-2 and DNA protein respectively, $\bar{\mu}_1$ is the rate of transcription of HMGCR mRNA and $\bar{\mu}_3$ is the rate of HMGCR translation. Finally x_h is the number of binding sites on the DNA that SREBP-2 must bind to.

Binding of SREBP-2 to squalene synthase DNA and subsequent mRNA and protein formation is governed by

$$
G_{ss} + x_s S \;\; \underset{\bar{\kappa}_{-2}}{\overset{\bar{\kappa}_2}{\rightleftharpoons}} \;\; S_{bss} \;\; \overset{\bar{\mu}_2}{\longrightarrow} \;\; M_{ss} \;\; \overset{\bar{\mu}_4}{\longrightarrow} \;\; S_s, \qquad (A.2)
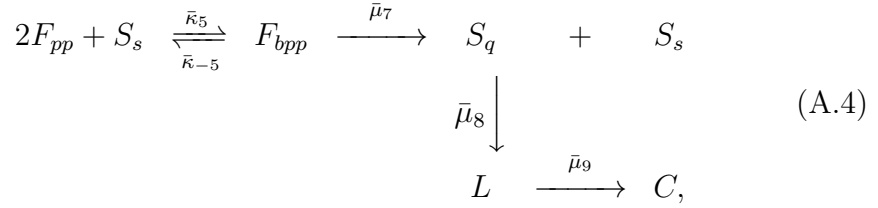$$

where free DNA binding sites responsible for squalene synthase synthesis is represented by G_{ss}, S_{bss} is SREBP-2 bound to the DNA, M_{ss} is squalene synthase mRNA and S_s is squalene synthase. The constant reaction rates $\bar{\kappa}_2$ and $\bar{\kappa}_{-2}$ represent the binding and unbinding of SREBP-2 and DNA respectively, $\bar{\mu}_2$ is the rate of transcription of mRNA responsible for squalene synthase and $\bar{\mu}_4$ is the rate of translation of squalene synthase from mRNA. Finally x_s is the number of binding sites on the DNA that SREBP-2 must bind to.

Binding of HMGCR and HMGCoA and subsequent production of geranyl-PP and farnesyl-PP is governed by

$$
H_r + H_c \;\; \underset{\bar{\kappa}_{-4}}{\overset{\bar{\kappa}_4}{\rightleftharpoons}} \;\; H_b \;\; \overset{\bar{\mu}_5}{\longrightarrow} \;\; G_{pp} \;\; + \;\; H_r,
$$
$$
\bar{\mu}_6 \downarrow \qquad\qquad\qquad (A.3)
$$
$$
F_{pp}
$$

42

where free HMGCoA is represented by H_c, H_b is HMGCR bound to HMG-CoA, G_{pp} is geranyl-PP and F_{pp} is farnesyl-PP. The constant reaction rates $\bar{\kappa}_4$ and $\bar{\kappa}_{-4}$ represent binding and unbinding of HMGCR and HMGCoA respectively, $\bar{\mu}_5$ is the rate of production of geranyl-PP and $\bar{\mu}_6$ is the rate of production of farnesyl-PP.

Two molecules of farnesyl-PP bind to one molecule of squalene synthase for the subsequent production of squalene, lanosterol and cholesterol such that

$$2F_{pp} + S_s \underset{\bar{\kappa}_{-5}}{\overset{\bar{\kappa}_5}{\rightleftharpoons}} F_{bpp} \xrightarrow{\bar{\mu}_7} S_q \quad + \quad S_s$$
$$\bar{\mu}_8 \downarrow \qquad \qquad \text{(A.4)}$$
$$L \xrightarrow{\bar{\mu}_9} C,$$

where bound farnesyl-PP and squalene synthase is represented by F_{bpp}, S_q is squalene, L is lanosterol and C is cholesterol. The constant reaction rates $\bar{\kappa}_5$ and $\bar{\kappa}_{-5}$ denote binding and unbinding of squalene synthase and farnesyl-PP respectively, $\bar{\mu}_7$ is the rate of squalene production, $\bar{\mu}_8$ is the rate of lanosterol production $\bar{\mu}_9$ that of cholesterol.

The negative regulation of SREBP-2 by cholesterol is governed by

$$x_c C + S \underset{\bar{\kappa}_{-3}}{\overset{\bar{\kappa}_3}{\rightleftharpoons}} C_b, \qquad \qquad \text{(A.5)}$$

where bound cholesterol and SREBP-2 is represented by C_b, the constant reaction rates $\bar{\kappa}_3$ and $\bar{\kappa}_{-3}$ represent the binding and unbinding of cholesterol and SREBP-2, respectively. Finally x_c is the number of binding sites that must be occupied by cholesterol on SREBP-2 to inactivate SREBP-2.

Each degradation process is described by

$$M_h \xrightarrow{\bar{\delta}_1} \phi, \quad M_{ss} \xrightarrow{\bar{\delta}_2} \phi, \quad H_r \xrightarrow{\bar{\delta}_3} \phi, \quad S_s \xrightarrow{\bar{\delta}_4} \phi,$$
$$G_{pp} \xrightarrow{\bar{\delta}_5} \phi, \quad F_{pp} \xrightarrow{\bar{\delta}_6} \phi, \quad L \xrightarrow{\bar{\delta}_7} \phi, \quad C \xrightarrow{\bar{\delta}_8} \phi,$$
$$\text{(A.6)}$$
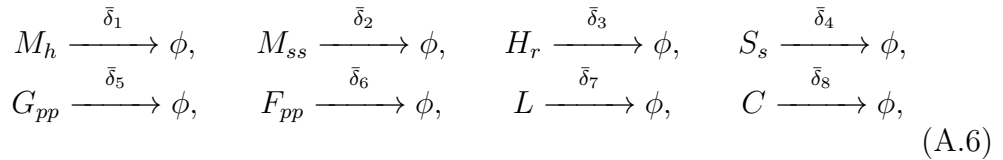
where δ_i ($i \in [1, ..., 8]$) are the rates of degradation of each mRNA, protein and enzyme, respectively.

Appendix B. Model reduction

We begin by observing three conservation relations. Firstly, the total amount
of DNA within a cell remains constant such that

$$\bar{g}_h + \bar{s}_{bh} = \bar{g}_{h0} \quad \text{and} \quad \bar{g}_{ss} + \bar{s}_{bss} = \bar{g}_{ss0}, \tag{B.1}$$

which are formed from the addition and integration (with respect to time)
of equations (1) and (4) , and (2) and (5), respectively.

The total amount of SREBP-2 in a cell is also constant which similarly gives

$$\bar{s} + \bar{c}_b = \bar{s}_0, \tag{B.2}$$

using equations (3) and (18).

We assume the following reactions occur on a faster timescale than others in
the signalling cascade and as such invoke the quasi-steady-state approxima-
tion. We assume DNA-transcription factor binding is rapid [20, 2] such that
from equation (4)

$$\bar{\kappa}_1 \bar{s}^{x_h}\left(\bar{g}_{h0} - \bar{s}_{bh}\right) - \bar{\kappa}_{-1}\bar{s}_{bh} \approx 0,$$

where we have substituted for $\bar{g}_h$ using the first conservation relationship in
equation (B.1). This result can be re-arranged for $\bar{s}_{bh}$ to give

$$\bar{s}_{bh} \approx \frac{\bar{g}_{h0}\bar{s}^{x_h}}{\bar{s}^{x_h} + \bar{K}_1^{x_h}}, \tag{B.3}$$

with $\bar{K}_1 = \left(\frac{\bar{\kappa}_{-1}}{\bar{\kappa}_1}\right)^{\frac{1}{x_h}}$.

Using the second conservation relationship in equation (B.1) and applying
the same assumption to equation (5) yields

$$\bar{s}_{bss} \approx \frac{\bar{g}_{ss0}\bar{s}^{x_s}}{\bar{s}^{x_s} + \bar{K}_2^{x_s}}, \tag{B.4}$$

with $\bar{K}_2 = \left(\frac{\bar{\kappa}_{-2}}{\bar{\kappa}_2}\right)^{\frac{1}{x_s}}$.

Finally we assume that cholesterol-SREBP-2 binding is also rapid such that
from equation (3)

$$\bar{s} \approx \frac{\bar{K}_3^{x_c}\bar{s}_0}{\bar{c}^{x_c} + \bar{K}_3^{x_c}} = \frac{\bar{s}_0}{1 + (\frac{\bar{c}}{\bar{K}_3})^{x_c}}, \tag{B.5}$$

with $\bar{K}_3 = \left(\frac{\bar{\kappa}_{-3}}{\bar{\kappa}_3}\right)^{\frac{1}{x_c}}$. This relationship can subsequently be used to express $\bar{s}_{bh}$ and $\bar{s}_{bss}$ in terms of c.

Using the results of equations (B.3), (B.4) and (B.5) we can simplify equations (6) and (7) to

$$\frac{d\bar{m}_h}{d\bar{t}} = \frac{\bar{\mu}_1^*}{1 + \left(\frac{\bar{K}_1(1+(\frac{\bar{c}}{\bar{K}_3})^{x_c})}{\bar{s}_0}\right)^{x_h}} - \bar{\delta}_1 \bar{m}_h, \tag{B.6}$$

and

$$\frac{d\bar{m}_{ss}}{d\bar{t}} = \frac{\bar{\mu}_2^*}{1 + \left(\frac{\bar{K}_2(1+(\frac{\bar{c}}{\bar{K}_3})^{x_c})}{\bar{s}_0}\right)^{x_s}} - \bar{\delta}_2 \bar{m}_{ss}, \tag{B.7}$$

where $\bar{\mu}_1^* = \bar{\mu}_1 \bar{g}_{h0}$ and $\bar{\mu}_2^* = \bar{\mu}_2 \bar{g}_{ss0}$.

Equation (31) is derived from equations (3), (4), (5) and (17), respectively, such that

$$\frac{d}{d\bar{t}}(\bar{s} + x_h \bar{s}_{bh} + x_s \bar{s}_{bss} - \bar{c}/x_c) = \frac{\bar{\mu}_9 \bar{l} - \bar{\delta}_8 \bar{c}}{x_c}$$

which leads to

$$(1 - x_c(\bar{s}' + x_h \bar{s}'_{bh} + x_s \bar{s}'_{bss}))\frac{d\bar{c}}{d\bar{t}} = \bar{\mu}_9 \bar{l} - \bar{\delta}_8 \bar{c},$$

via the chain rule, where $'$ denotes differentiation with respect to $\bar{c}$ such that from (B.5), (B.3) and (B.4) we have

$$\frac{d\bar{s}}{d\bar{c}} = \frac{-\bar{s}_0 x_c \left(\frac{\bar{c}}{\bar{K}_3}\right)^{x_c}}{\bar{c}\left(1 + \left(\frac{\bar{c}}{\bar{K}_3}\right)^{x_c}\right)^2}, \tag{B.8}$$

$$\frac{d\bar{s}_{bh}}{d\bar{c}} = \frac{d\bar{s}_{bh}}{d\bar{s}}\frac{d\bar{s}}{d\bar{c}} = \frac{x_h \bar{g}_{h0} \bar{K}_1^{x_h} \bar{s}^{x_h - 1}}{(\bar{s}^{x_h} + \bar{K}_1^{x_h})^2}\frac{d\bar{s}}{d\bar{c}} \tag{B.9}$$

and

$$\frac{d\bar{s}_{bss}}{d\bar{c}} = \frac{d\bar{s}_{bss}}{d\bar{s}}\frac{d\bar{s}}{d\bar{c}} = \frac{x_s \bar{g}_{ss0} \bar{K}_2^{x_s} \bar{s}^{x_s - 1}}{(\bar{s}^{x_s} + \bar{K}_2^{x_s})^2}\frac{d\bar{s}}{d\bar{c}}, \tag{B.10}$$

respectively. Here $\bar{g}_{h0}$ and $\bar{g}_{ss0}$ are the total concentration of HMGCR and squalene synthase DNA, respectively, in a cell.

45

Appendix C. Parameter details

In this section we detail, where relevant, calculations used to estimate the parameters detailed in Table 1.

$\bar{\mathbf{m}}_{\mathbf{h0}}$ **- Initial concentration of HMGCR mRNA**: Ruddling et al. [30] details copy numbers of mRNA found in human liver cells under basal conditions. So we take a value of 30 copies of HMGCR mRNA per cell i.e. per 10^{-9} ml. So

$$\frac{30 \text{ molecules}}{1 \times 10^{-9}\text{ml}} = 3.0 \times 10^{10} \text{ molecules/ml.}$$

This value was then refined using local sensitivity analysis to give $\bar{m}_{h0} = 3.0 \times 10^9$ molecules/ml.

$\bar{\mathbf{m}}_{\mathbf{ss0}}$ **- Initial concentration of squalene synthase mRNA**: Ruddling et al. [30] details copy numbers of mRNA found in human liver cells under basal conditions. So we take a value of 30 copies of squalene synthase mRNA per cell i.e. per 10^{-9} ml. So

$$\frac{30 \text{ molecules}}{1 \times 10^{-9}\text{ml}} = 3.0 \times 10^{10}\text{molecules/ml.}$$

This value was then refined using local sensitivity analysis to give $\bar{m}_{ss0} = 3.0 \times 10^9$ molecules/ml.

$\bar{\mathbf{s}}_{\mathbf{sT}}$ **- Total concentration of squalene synthase**: One liver cell contains 300pg/cell protein and has a volume of 10^{-9} ml. Bruenger and Rilling [5] state there are 4.2 nmol of squalene synthase per gram of wet tissue such that

$$4.2 \times 10^{-9}\text{mol/g tissue} \times 6.022 \times 10^{23} \text{ molecules/mol}$$

which gives

$$\frac{2.53 \times 10^{15}\text{molecules /g} \times 1.00 \times 10^{-12}}{10^{-9}\text{ml}} = 7.59 \times 10^{14} \text{ molecules/ml.}$$

$\bar{\mathbf{h}}_{\mathbf{cT}}$ **- Total concentration of HMGCoA**: One liver cell contains approximately 300pg/cell protein and has volume 10^{-9}ml/cell. The molecular weight of HMGCoA is 199.659 g/mol according to human metabolic database [38]. Then we know

$$\frac{300 \times 10^{-12}\text{g}}{199.659\text{g/mol}} = 3.29 \times 10^{-13}\text{mol/cell.}$$

So we have, per cell, 3.29×10^{-13}mol/10^{-9}ml $= 3.92 \times 10^{-4}$ mol/ml. Applying Avagadro's number we can find the number of molecules per ml

$$3.92 \times 10^{-4} \text{ mol/ml } \times 6.022 \times 10^{23} \text{ molecules/mol } = 1.98 \times 10^{20} \text{ molecules/ml.}$$

Segel (1993) [33] states a cell contains an average of 1000 enzymes, so we have 9.04×10^{14} molecules/ml. This value was then refined using local sensitivity analysis to give $\bar{h}_{cT} = 1.98 \times 10^{15}$ molecules/ml.

$\bar{\mathbf{g}}_{\mathbf{h0}}, \bar{\mathbf{g}}_{\mathbf{ss0}}$ - **HMGCR and squalene synthase gene concentration**: The molecular weight of the HMGCR gene is 97,476 Da [41], whilst that of the human genome is 2×10^{12}Da [42]. The total quantity of DNA in a cell weighs 7pg, such that that of HMGCR is 3.41×10^{-7}pg. Observing that 1 Da is equivalent to 1g/mol and assuming the volume of a cell is 1 nml, we have

$$\frac{3.41 \times 10^{-7} \text{ pg} \times 6.023 \times 10^{23} \text{ molecules/mol}}{97,476 \text{ g/mol } \times 1 \text{ nml}} = 2.11 \times 10^{9} \text{molec/ml.}$$

We likewise assume the squalene synthase gene (with no further details available) is the same concentration.

$\bar{\mu}_1^*$ - **Rate of HMGCR mRNA transcription**: Darzacq et al. [8] states 12 bases are transcribed per second. Goldstein and Brown [12] say one HMGCoA-R gene is 24826 bases long. Therefore we have

$$\frac{24826 \text{ bases}}{12 \text{ bases/s}} = 2068.83\text{s.}$$

We add 30 minutes to account for post transcriptional processing steps of mRNA cleavage giving 3868.83s. So for one gene we have

$$\frac{1 \text{ molecule}}{3868.83\text{s}} = 2.58 \times 10^{-4} \text{ molecules/s.}$$

A liver cell is somatic and hence diploid meaning it contains contains two genes, so we have

$$2.58 \times 10^{-4} \text{ molecules/s} \times 2 = 5.17 \times 10^{-4} \text{molecules/s.}$$

The average cell volume is 1pl $= 1 \times 10^{-9}$ml so the rate of transcription is given by

$$\frac{5.17 \times 10^{-4} \text{ molecules/s}}{1 \times 10^{-9}\text{ml}}$$

giving $\bar{\mu}_1^* = 5.17 \times 10^5$ molecules/ml/s.

$\bar{\mu}_2^*$ **- Rate of squalene synthase mRNA transcription**: Darzacq et al. [8] states 12 base pairs are transcribed per second. Tansey & Shechter [37] say one human squalene synthase gene is over 30000 bases long. Therefore we have

$$\frac{30000 \text{ bases}}{12 \text{ bases/s}} = 2500\text{s}.$$

We add 30 minutes to account for post transcriptional processing steps of mRNA cleavage giving 4300 thus for one gene we have

$$\frac{1 \text{ molecule}}{4300\text{s}} = 2.33 \times 10^{-4} \text{ molecules/s}.$$

A liver cell is somatic and hence diploid meaning it contains contains two genes, so we have

$$2.33 \times 10^{-4} \text{ molecules/s} \times 2 = 4.65 \times 10^{-4} \text{ molecules/s}.$$

The average cell volume is 1pl $= 1 \times 10^{-9}$ml so the rate of transcription is given by

$$\frac{4.65 \times 10^{-4} \text{ molecules/s}}{1 \times 10^{-9}\text{ml}}$$

giving $\bar{\mu}_2^* = 4.65 \times 10^5$ molecules/ml/s.

$\bar{\mu}_3$ **- Rate of HMGCR translation**: Trachsel [39] states 6 amino acids are translated per second. One amino acid is encoded by 3 bases or nucleotides. HMGCR mRNA transcript has 4475 bases (Goldstein & Brown [12]). Hence transcription takes:

$$\frac{4475 \text{ bases}}{6 \text{ amino acids/s} \times 3 \text{ amino acids/base}} = 248.61s,$$

We add 60 minutes to account for the initiation of this process

$$3848.61\text{s}.$$

Then per ribosome we have

$$\frac{1 \text{ molecule}}{3848.61\text{s}} = 2.60 \times 10^{-4} \text{ molecules/s/ribosome}.$$

A ribosome can only attach every 35 bases do to its size meaning 1 mRNA molecule has 127.86 ribosomes attached.

Then per mRNA molecule we have:

$$2.60 \times 10^{-4} \text{ molecules/s/ribosome} \times 127.86 \text{ ribosomes/molecule}$$

giving $\bar{\mu}_3 = 3.32 \times 10^{-2}$ /s.

$\bar{\mu}_4$ - **Rate of squalene synthase translation**: Trachsel [39] states 6 amino acids are translated per second. One amino acid is encoded by 3 bases or nucleotides. Jiang et al. [36] state that one squalene synthase mRNA transcript contains 2502 bases. Hence transcription takes:

$$\frac{2502 \text{ bases}}{6 \text{ amino acids/s} \times 3 \text{ amino acids/base}} = 139\text{s},$$

We add 60 minutes to account for the initiation of this process

$$3739\text{s}.$$

Then per ribosome we have

$$\frac{1 \text{ molecule}}{3739\text{s}} = 2.67 \times 10^{-4} \text{ molecules/s/ribosome}.$$

A ribosome can only attach every 35 bases do to its size meaning 1 mRNA molecule has 71.49 ribosomes attached.

Then per mRNA molecule we have:

$$2.67 \times 10^{-4} \text{ molecules/s/ribosome} \times 71.49 \text{ ribosome/molecule}$$

giving $\bar{\mu}_4 = 1.91 \times 10^{-2}$ /s.

$\bar{\mu}_5$ - **Rate of geranyl-PP synthesis**: Tanaka et al. [47] tell us that liver microsomes form 52 pmol mevalonate per minute per mg protein. Istvan et al. [15] say HMGCR is tetrameric arranged in 2 dimer, with 4 active sites, has molecular weight 199812 Da. The activity of the enzyme is where

$$52 \times 10^{-12} \text{mol/min/mg protein} \approx 52 \times 10^{-12} \times N_A.$$

$N_A = 6.022 \times 10^{23}$ is Avagadro's constant. So we have

$$52 \times 10^{-12} \text{mol/min/mg protein} \times 6.022 \times 10^{23} \text{ molecules/mol}$$

49

$$= 3.13 \times 10^{13} \text{ molecules/min/mg protein.}$$

Segel [33] says there's 1000 different enzymes in a cell, so for 1 mg of protein we have

$$\frac{1 \times 10^{-3}\text{g}}{199812\text{g/mol} \times 1000} = 5.00 \times 10^{-12}\text{mol.}$$

Given there are 4 active sites per HMGA-CoA Reductase enzyme, there are 2.00×10^{-11} moles of enzyme active sites in 1 mg of protein. Given the specific activity of an enzyme we find $\bar{\mu}_5$ is equal to

$$\frac{52 \times 10^{-12} \text{ mol/min/mg}}{2.00 \times 10^{11}\text{mol/mg}} = 2.60\text{min}$$

giving $\bar{\mu}_5 = 4.33 \times 10^{-2}$/s.

$\bar{\mu}_6$, $\bar{\mu}_8$ and $\bar{\mu}_9$ - Rates of farnesyl-PP, lanosterol and cholesterol synthesis: Since the value for $\bar{\mu}_5$ is used to describe cholesterol production from HMGCR, we can assume all steps in between must occur at the same rate or faster. Therefore we set $\bar{\mu}_6$, $\bar{\mu}_8$ and $\bar{\mu}_9$ equal to 4.33×10^{-2} /s.

$\bar{\mu}_7$ - Rate of squalene synthesis. Since the value for $\bar{\mu}_5$ is used to describe cholesterol production from HMGCR, we can assume all steps in between must occur at the same rate or faster. Therefore as an estimate we set $\bar{\mu}_7$ equal to 4.33×10^{-2} /s. This value was then refined using local sensitivity analysis to give $\bar{\mu}_7 = 2.17 \times 10^{-1}$ 1/s.

$\bar{K}_1$ - Disassociation constant of SREBP-2 for HMGCR DNA: Yang and Swartz [29] quantifed DNA binding affinities to other transcription factors at 54.2 nmol. We convert this value into units of molecules/ml by the use of Avogadro's constant.

$$\frac{100 \times 10^{-9} \text{ moles}}{1000\text{ml}} \times 6.022 \times 10^{23} \text{ molecules/mol} = 3.26 \times 10^{13} \text{ molecules/ml.}$$

This value was then refined using local sensitivity analysis to give $\bar{K}_1 = 8.21 \times 10^{12}$ molecules/ml.

$\bar{K}_2$ - Disassociation constant of SREBP-2 for squalene synthase DNA: This was assumed equivalent to that of SREBP-2 for HMGCR DNA, i.e. 3.26×10^{13} molecules/ml. The value was then refined using local sensitivity analysis to give $\bar{K}_2 = 8.21 \times 10^{12}$ molecules/ml.

$\bar{K}_3$- Disassociation constant of SREBP-2 for cholesterol: Radhakrishnan et al. [46] state the binding reaction between cholesterol and SCAP is saturable and half-maximal binding occurs at approximately 100 nmol. We convert this value into units of molecules/ml by the use of Avogadro's constant.

$$\frac{100 \times 10^{-9} \text{ moles}}{1000 \text{ ml}} \times 6.022 \times 10^{23} \text{ molecules/mol} = 6.02 \times 10^{13} \text{ molecules/ml},$$

as an estimate we took $\bar{K}_3 = O(10^{14})$. This value was then refined using local sensitivity analysis to give $\bar{K}_3 = 1.49 \times 10^{16}$ molecules/ml.

$\bar{\kappa}_4$ and $\bar{\kappa}_{-4}$ - Forward and reverse rates of HMGCR binding to HMG-CoA: These values were initially informed by assuming the ratio of $\bar{\kappa}_4/\bar{\kappa}_{-4}$ were the same order as those of $\bar{K}_1$, $\bar{K}_2$ and $\bar{K}_3$. We then assumed $\bar{\kappa}_{-4} \ll \bar{\kappa}_4$ whereby we took an initial estimate of $\bar{\kappa}_{-4} = 1 \times 10^{-3}$/s. These values were then adjusted, via a sensitivity analysis, to give the required steady-state cholesterol levels. This resulted in values of $\bar{\kappa}_4 = 1.39 \times 10^{-16}$ ml/molecules s and $\bar{\kappa}_{-4} = 1.75 \times 10^{-7}$ /s.

$\bar{\kappa}_5/\bar{\kappa}_5$- Forward and reverse rates of farnesyl-PP binding to squalene synthase: These values were obtained in a similar manner to those of $\bar{\kappa}_4$ and $\bar{\kappa}_{-4}$. This led to $\bar{\kappa}_5 = 1.76 \times 10^{-30}$ ml/molecule s and $\bar{\kappa}_{-5} = 1.75 \times 10^{-5}$ /s.

$\bar{K}_6$, $\bar{K}_7$, $\bar{K}_8$, $\bar{K}_9$ and $\bar{K}_{10}$ - Michaelis-Menten constants of geranyl-PP, farnesyl-PP, lanosterol and cholesterol for HMGCR degradation and cholesterol for squalene synthase degradation, respectively: These were determined as the half-maximal values which produced a sigmoidal type response for each of the respective cascade products.

$\bar{\delta}_1$- Degradation rate of HMGCR mRNA. Degradation rates of proteins and mRNAs are based on their half lives, derived from an exponential decay model. Wilson and Deeley [3] state HMGCR mRNA has a half life of 4.3 hours, measured in Hep G2 cells, giving $\bar{\delta}_1 = \ln 2/15480 \text{s} = 4.48 \times 10^{-5}$/s.

$\bar{\delta}_2$ - Degradation rate of squalene synthase mRNA: This was assumed equivalent to that of HMGCR mRNA.

$\bar{\delta}_3$ - Degradation of HMGCR: Brown et al. [44] found HMGCR protein has a half life of 3 hours, measured in human fibroblast cells, such that $\bar{\delta}_3 = \ln 2/10800 s = 6.42 \times 10^{-5}$/s.

$\bar{\delta}_4$ **- Squalene synthase degradation rate**: This was assumed equivalent to that of HMGCR.

$\bar{\delta}_5$, $\bar{\delta}_6$ and $\bar{\delta}_7$ **- Degradation rates of geranyl-PP, farnesyl-PP and lanosterol:** These were assumed equivalent to that of cholesterol.

$\bar{\delta}_8$ **- Cholesterol degradation rate**: We utilise the value previously derived in Bhattacharya et al. [2] of 1.20×10^{-4}/s.

$\bar{\omega}$ **- HMGCoA production rate**: This value has been determined from our sensitivity analysis to be 3.895×10^{11}molec./ml. The value has been found to ensure enough cholesterol is produced.

$\mathbf{x_h}$ **- Number of binding sites for SREBP-2 on HMGCR DNA**: Vallett et al. [28] state a value of 3.

$\mathbf{x_s}$ **- Number of binding sites for SREBP-2 on squalene synthase DNA**: Without further evidence we assume this is 1.

$\mathbf{x_c}$ **- Number of binding sites on SREBP-2 for cholesterol**: Radhakrishnan et al. [46, 16] state a value of 4.

References

[1] August, E., Parker, K., Barahona, M., 2007. A dynamical model of lipoprotein metabolism. Bulletin of Mathematical Biology 69 (4), 1233–1254.

[2] Bhattacharya, B., Sweby, P., Minihane, A.-M., Jackson, K., Tindall, M., 2014. A mathematical model of the sterol regulatory element binding protein 2 cholesterol biosynthesis pathway. Journal of Theoretical Biology 349, 150–162.

[3] Brown, M., Dana, S., Goldstein, J., 1974. Regulation of 3-hydroxy-3-methylglutaryl coenzyme A reductase activity in cultured human fibroblasts comparison of cells from a normal subject and from a patient with homozygous familial hypercholesterolemia. Journal of Biological Chemistry 249 (3), 789–796.

[4] Brown, M., Goldstein, J., 1980. Multivalent feedback regulation of HMG CoA reductase, a control mechanism coordinating isoprenoid synthesis and cell growth. Journal of Lipid Research 21 (5), 505–517.

[5] Bruenger, E., Rilling, H., 1988. Determination of isopentenyl diphosphate and farnesyl diphosphate in tissue samples with a comment on secondary regulation of polyisoprenoid biosynthesis. Analytical Biochemistry 173 (2), 321–327.

[6] Buhaescu, I., Izzedine, H., 2007. Mevalonate pathway: a review of clinical and therapeutical implications. Clinical Biochemistry 40 (9), 575–584.

[7] Cole, S., Vassar, R., 2006. Isoprenoids and alzheimer's disease: A complex relationship. Neurobiology of Disease 22, 209–222.

[8] Darzacq, X., Shav-Tal, Y., de Turris, V., Brody, Y., Shenoy, S., Phair, R., Singer, R., 2007. In vivo dynamics of RNA polymerase II transcription. Nature Structural & Molecular Biology 14 (9), 796–806.

[9] DeBose-Boyd, R., 2008. Feedback regulation of cholesterol synthesis: sterol-accelerated ubiquitination and degradation of hmg coa reductase. Cell Research 18, 609–21.

[10] Foresti, O., Ruggiano, A., Hannibal-Bach, H., Ejsing, C., Carvalho, P., 2013. Sterol homeostasis requires regulated degradation of squalene monooxygenase by the ubiquitin ligase Doa10/Teb4. Elife 2, e00953.

[11] Gaylor, J. L., 2002. Membrane-bound enzymes of cholesterol synthesis from lanosterol. Biochemical and biophysical research communications 292 (5), 1139–1146.

[12] Goldstein, J., Brown, M., 1984. Progress in understanding the LDL receptor and HMG-CoA reductase, two membrane proteins that regulate the plasma cholesterol. Journal of Lipid Research 25 (13), 1450–1461.

[13] Goldstein, J., Brown, M., 1990. Regulation of the mevalonate pathway. Nature 343 (6257), 425–30.

[14] Hampton, R., 2002. Proteolysis and sterol regulation. Annual Review of Cell and Developmental Biology 18, 345–78.

[15] Istvan, E., Palnitkar, M., Buchanan, S., Deisenhofer, J., 2000. Crystal structure of the catalytic portion of human HMG-CoA reductase: insights into regulation of activity and catalysis. The EMBO Journal 19 (5), 819–830.

[16] Jackson, K., Maitin, V., Leake, D., Yaqoob, P., Williams, C., 2006. Saturated fat-induced changes in Sf 60–400 particle composition reduces uptake of LDL by HepG2 cells. Journal of Lipid Research 47 (2), 393–403.

[17] Jiang, G., McKenzie, T., Conrad, D., Shechter, I., 1993. Transcriptional regulation by lovastatin and 25-hydroxycholesterol in HepG2 cells and molecular cloning and expression of the cDNA for the human hepatic squalene synthase. Journal of Biological Chemistry 268 (17), 12818–12824.

[18] Kellner-Weibel, G., Geng, Y., Rothblat, G., 1999. Cytotoxic cholesterol is generated by the hydrolysis of cytoplasmic cholesteryl ester and transported to the plasma membrane. Atherosclerosis 146, 309–19.

[19] Kervizic, G., Corcos, L., 2008. Dynamical modeling of the cholesterol regulatory pathway with boolean networks. BMC Systems Biology 2 (99), doi: 10.1186/1752–0509–2–99.

[20] Lickwar, C. R., Mueller, F., Hanlon, S. E., McNally, J. G., Lieb, J. D., 2012. Genome-wide protein-DNA binding dynamics suggest a molecular clutch for transcription factor function. Nature 484 (7393), 251–255.

[21] Matlab, Release 2016b. The MathWorks. Natick, Massachusetts, United States.

[22] Mazein, A., Watterson, S., Hsieh, W., WJ, G., P, G., 2013. A comprehensive machine-readable view of the mammalian cholesterol biosynthesis pathway. Biochemical Pharmacology 86 (1), 56–66.

[23] Menegola, E., Broccia, M., Di Renzo, F., E, G., 2006. Postulated pathogenic pathway in triazole fungicide induced dysmorphogenic effects. Reproductive Toxicology 260 (2), 186–95.

[24] Michaelis, L., Menten, M., 1913. Die kinetik der invertinwirkung. Biochemische Zeitschrift 49 (333-369), 352.

[25] Morgan, A., Mooney, K., Wilkinson, S., Pickles, N., MT., M. A., 2016. Mathematically modelling the dynamics of cholesterol metabolism and ageing. Biosystems 145, 19–32.

[26] Murphy, L., Moore, T., S, N., 2012. Propiconazole-enhanced hepatic cell proliferation is associated with dysregulation of the cholesterol biosynthesis pathway leading to activation of Erk1/2 through Ras farnesylation. Toxicology and Applied Pharmacology 260 (2), 146–54.

[27] Murray, J., 2002. Mathematical Biology I: An Introduction. Springer, New York, USA.

[28] Radhakrishnan, A., Goldstein, J., McDonald, J., Brown, M., 2008. Switch-like control of SREBP-2 transport triggered by small changes in ER cholesterol: a delicate balance. Cell Metabolism 8 (6), 512–521.

[29] Radhakrishnan, A., Sun, L.-P., Kwon, H., Brown, M., Goldstein, J., 2004. Direct binding of cholesterol to the purified membrane region of SCAP: mechanism for a sterol-sensing domain. Molecular Cell 15 (2), 259–268.

[30] Rudling, M., Angelin, B., Ståhle, L., Reihnér, E., Sahlin, S., Olivecrona, H., Björkhem, I., Einarsson, C., 2002. Regulation of hepatic low-density lipoprotein receptor, 3-hydroxy-3-methylglutaryl coenzyme A reductase, and cholesterol 7α-hydroxylase mRNAs in human liver. The Journal of Clinical Endocrinology & Metabolism 87 (9), 4307–4313.

[31] Sanguinetti, G., Lawrence, N., Rattray, M., 2006. Probabilistic inference of transcription factor concentrations and gene-specific regulatory activities. Bioinformatics 22 (22), 2775–2781.

[32] Sebti, S., Hamilton, A., 1997. Inhibition of Ras prenylation: A novel approach to cancer chemotherapy. Pharmacology and Therapeutics 74 (1), 103–114.

[33] Segal, I., 1975. Enzyme kinetics behaviour and analysis of rapid equilibrium and steady-state enzyme systems. A Wiley-Interscience Publication, New York, USA.

[34] Siperstein, M., Fagan, V., 1966. Feedback control of mevalonate synthesis by dietary cholesterol. Journal of Biological Chemistry 241 (3), 602–609.

[35] Srivastava, R., Ito, H., Hess, M., Srivastava, N., Schonfeld, G., 1995. Regulation of low density lipoprotein receptor gene expression in HepG2

and Caco2 cells by palmitate, oleate, and 25-hydroxycholesterol. Journal of lipid research 36 (7), 1434–1446.

[36] Tanaka, R., Edwards, P., Lan, S., Knöppel, E., Fogelman, A., 1982. Purification of 3-hydroxy-3-methylglutaryl coenzyme A reductase from human liver. Journal of Lipid Research 23 (4), 523–530.

[37] Tansey, T., Shechter, I., 2000. Structure and regulation of mammalian squalene synthase. Biochimica et Biophysica Acta-Molecular and Cell Biology of Lipids 1529 (1), 49–62.

[38] The Metabolomics Innovation Centre, Accessed: 31-07-2015. The human metabolome database. `http://www.hmdb.ca/metabolites/HMDB01375`.

[39] Trachsel, H., 1991. Translation in eukaryotes. CRC Press, Florida, USA.

[40] Turley, S., Dietschy, J., 2003. The intestinal absorption of biliary and dietary cholesterol as a drug target for lowering the plasma cholesterol level. Preventive Cardiology 6 (1), 29–64.

[41] Cards, G., Accessed: 15-10-2017. Hmgcr gene size. `http://www.genecards.org/cgi-bin/carddisp.pl?gene=HMGCR`.

[42] DNA technologies, I., Accessed: 17-10-2017. Molecular facts and figures. `https://www.idtdna.com/pages/docs/educational-resources/molecular-facts-and-figures.pdf?sfvrsn=4`.

[43] van Greevenbroek, M., de Bruin, T., 1998. Chylomicron synthesis by intestinal cells in vitro and in vivo. Atherosclerosis 141, S9–S16.

[44] Vargas, N., Brewer, B., Rogers, T., Wilson, G., 2009. Protein kinase C activation stabilizes LDL receptor mRNA via the JNK pathway in HepG2 cells. Journal of Lipid Research 50 (3), 386–397.

[45] Watterson, S., Guerriero, M., Blanc, M., Mazein, A., Loewe, L., Robertson, K., Gibbs, H., Shui, G., Wenk, M., Hillston, J., P., G., 2013. A model of flux regulation in the cholesterol biosynthesis pathway: Immune mediated graduated flux reduction versus statin-like led stepped flux reduction. Biochimie 95 (3), 613–21.

[46] Wilson, G., Deeley, R., 1995. An episomal expression vector system for monitoring sequence-specific effects on mRNA stability in human cell lines. Plasmid 33 (3), 198–207.

[47] Yang, W., Swartz, J., 2011. A filter microplate assay for quantitative analysis of DNA binding proteins using fluorescent DNA. Analytical Biochemistry 415 (2), 168–174.